The effect of the liquid physical properties on the wave frequency and wave velocity of co-current gas-liquid stratified two-phase flow in a horizontal pipe

Setya Wijayanta [a,b], Deendarlianto [a,c,*], Indarto [a,c], Ari Prasetyo [a], Akhmad Zidni Hudaya [d]

[a] Department of Mechanical and Industrial Engineering, Universitas Gadjah Mada, Jalan Grafika No. 2, Yogyakarta 55281, Indonesia
[b] Study Program of Authomotive Technology, Politeknik Keselamatan Transportasi Jalan, Jalan Semeru No. 3, Kota Tegal, Central Java 52125, Indonesia
[c] Centre for Energy Studies, Universitas Gadjah Mada, Skip K-1A, Kampus UGM, Yogyakarta 55281, Indonesia
[d] Department of Mechanical Engineering, Universitas Muria Kudus, Kudus, Central Java, Indonesia

ARTICLE INFO

ABSTRACT

The aim of the present study was to investigate the effect of the liquid physical properties on the liquid film thickness, wave frequency, and wave velocity in co-current gas-liquid stratified two-phase flow in a horizontal pipe. The present experimental study was conducted using an acrylic pipe with an inner diameter of 26 mm and a length of 9500 mm. The superficial velocity of liquid (J_L) and gas (J_G) were 0.02 m/s to 0.1 m/s and 4 m/s to 16 m/s, respectively. A highspeed video camera was used to take the visual data which is then processed by the developed image processing techniques to obtain the time series data of the liquid film thickness. The probability distribution function (PDF) and discrete wavelet transform (DWT) were used to analyze the time series of the liquid film thickness. In addition, the data were also analyzed using the power spectral density (PSD) in order to obtain the wave frequency and the wave velocity. Next, the experimental correlations to predict the wave frequency and the wave velocity were developed using the dimensional analysis. From the time series of the liquid film thickness, the effect of the viscosity and surface tension on the shifting of scale and frequency of the wavelet decomposition level, as well as the frequency and velocity of the waves were clarified. In addition, a correlation to predict the frequency and velocity of waves has been successfully developed, in which the Martinelli parameter, the ratio of gas and liquid Reynold numbers, and the Weber number play the important roles in the correlation.

1. Introduction

The horizontal stratified wavy flow is often found in oil and gas transportation systems. Under sufficiently high flow rates, waves in stratified flow grow with large enough amplitudes, one example being roll waves (Hanratty and Hershman, 1961). Under many flow conditions, the roll wave grows into slug form by other mechanisms (Lin and Hanratty, 1986). Roll wave and slug at lower levels cause the fluctuations in pressure and flow rate which can damage instrumentation (Bruno, 1988). In addition, Villarreal et al. (2006) stated that in the case of the production and transportation of hydrocarbons, the presence of slug flow causes the increase of the corrosion rate. Therefore, the operators and the design engineer of the piping system mostly avoid the occurrence of slug flow (Dinaryanto et al., 2017). Thus, many piping

systems are designed to operate in a stratified flow regime and avoid the slug.

Aydin et al. (2015) reported that in the natural gas pipelines, a gas-liquid stratified flow can be observed, whereas the condensation occurs during the transport of single-phase natural gas. In this situation, the interfacial waves play the important role in the process of mass, momentum, and energy transfer between the gas and liquid phases. This is in line with the report from McCready and Hanratty (1985), who explained that a measurable increase in mass transfer rate for non-sheared non-wavy interfaces could reach ten (10) times the mass transfer rate for wavy interfaces. Those are also in a good agreement with those of Lockhart and Martinelli (1949), Andritsos and Hanratty (1987), Kowalski (1987) and Al-Wahaibi and Angeli (2011) who suggested that the interface wave will affect the interface roughness

Table 1

The Summary of studies on the wave characteristics of gas-liquid two-phase flow in horizontal channels.

Researcher (Year)	Experimental Conditions	Regime	Measurement Method	Equation/Correlation
Mantilla, et al. (2009)	- Working fluid: air – (water + gliserin) for viscosity variations air – (water + butanol) for surface tension variations - Pipe diameter = 50.8 mm and 152.4 mm - J_G D = 50.8 mm (5 - 80 m/s), D = 152.4 mm (2 - 20 m/s)	Stratified - Annular	• liquid film thickness and wave parameters (conductance probe). • liquid film thickness < 4 mm (flush mounted conductance probe) • Thicker liquid film thickness (parallel conductance wire probes)	*Frequency* $St = 0.25\,X^{1.2}$ $St = \dfrac{fD}{J_L}$, $X = \sqrt{\dfrac{\rho_L}{\rho_G}\dfrac{J_L^2}{J_G^2}}$ *Velocity* $c_w = \dfrac{\psi J_G + J_L}{1 + \psi}$; $\psi = 5,5\sqrt{\dfrac{\rho_G}{\rho_L}}\left(\dfrac{\mu_L}{\mu_w}\dfrac{Re_{SL}}{Re_{SG}}\right)^{0.25}$ *Amplitude* $\dfrac{\Delta h_w}{h_L} = 1350\dfrac{Re_{SL}^{0.1}}{Re_{SG}^{0.5}} - 3.25$ *Wave spacing* $L_w = \dfrac{c_w}{f}$
Al Sarkhi, et al. [2011]	- J_L (0.0035 – 0.01 m/s) - Working fluid: water - air - Pipe diameter = 76.2 mm, pipe slope variation (0°, 10°, 20°, 45°, 60°, 75°, 90°) - J_G (40 – 80 m/s), J_L (0.0035-0.004 m/s)	Annular	• Liquid film thickness and wave parameter (flush mounted conductance probes) • Liquid holdup (quick-closing valves)	*Frequency* $St = 1.1X^{*-0.93}$ *Velocity* $\dfrac{c_w}{J_L} = 2.379X^{*-0.9}$
Gawas, et al. [2014]	- Working fluid: oil - air - Pipe diameter = 152.4 mm - J_G (10 – 23 m/s), J_L (0.005 – 0.02 m/s)	Stratified - Annular	Liquid film thickness and wave parameter (two wire capacitance sensor)	*Velocity* $\dfrac{c_w}{J_L} = 3.51X^{*-0.81}$, *for* $X^* < 0.305$ $\dfrac{c_w}{J_L} = 5.102X^{*-0.495}$, *for* $X^* > 0.305$ *Amplitude*, $\dfrac{\Delta h_w}{D} = 0.67\left(\dfrac{\Delta h_0}{D}\right)^{0.71}$ or $\dfrac{\Delta h_w}{D} = 0.58X^{0.53}$
Setyawan, et al. [2016]	- Working fluid: air - (water + glycerin) for viscosity variation air – (water + butanol) for surface tension variation - D. pipe 16 and 26 mm - J_G (12 – 40 m/s), J_L (0.05 – 0.2 m/s)	Annular	Liquid holdup and wave parameter (Constant-Electric Current Method/CECM)	*Frequency* $St = 0.258\left(\dfrac{\rho_L}{\rho_G}\right)^{0.574}\left(\dfrac{\mu_L}{\mu_G}\right)^{-1.148}\left(\dfrac{Re_L}{Re_{Gm}}\right)^{-1.148}\left(\dfrac{\sigma_L}{\sigma_w}\right)^{-0.11}$ *Velocity* $\dfrac{c_w}{J_L} = 7.25\left(\dfrac{\rho_L}{\rho_G}\right)^{0.35}\left(\dfrac{\mu_L}{\mu_G}\right)^{-0.7}\left(\dfrac{Re_L}{Re_{Gm}}\right)^{-0.7}\left(\dfrac{\sigma_L}{\sigma_w}\right)^{0.2}$ $Re_{Gm} = D\rho_G(J_G - J_L)/\mu_G$
Bae, et al. [2017]	- Water - Air - Rectangular channel (40 x 50 mm) - J_G (5 – 25 m/s), J_L (0.01 – 0.08 m/s)	Stratified	• Visualization (Particle Image Velocimetri and High Speed Camera) • Liquid flim thickness dan parameter gelombang (parallel wire conductance sensor)	*Frequency* $St = 0.057X^{-1.33} + 0.89$ *Amplitude* $\dfrac{\Delta h_w}{h_L} = 3.84exp\left[-\left(\dfrac{\dfrac{Re_{SL}^{0.1}}{Re_{SG}^{0.5}} - 0.0067}{0,0053}\right)^2\right]$ *for* $\dfrac{Re_{SL}^{0.1}}{Re_{SG}^{0.5}} \le 0,005$ *Velocity* $c_w = \dfrac{\psi J_G + J_L}{1 + \psi}$; $\psi = 5.5\sqrt{\dfrac{\rho_G}{\rho_L}}\left(\dfrac{Re_{SL}}{Re_{SG}}\right)^{0.25}$
Hudaya, et al. [2019]	- Water - Air - Pipe diameter 26 mm - J_G (4 – 16 m/s), J_L (0.02 – 0.075 m/s)	Stratified	• Visualization (high speed camera), • Liquid flim thickness and wave parameter (Image processing)	*Frequency* $St = 0.215\left[\dfrac{Re_{SG}}{Re_{SL}}\right]^{0.08}X^{-0.912}$ *Velocity* $c_w = 4.786J_L\left(\dfrac{Re_{SG}}{Re_{SL}}\right)^{0.18}X^{-0.51}$ *Amplitude* $\dfrac{\Delta h_w}{h_L} = 0.03\left(\dfrac{Re_{SG}}{Re_{SL}}\right)^{6.0}X^{5.7}$ *Long* $\dfrac{\lambda_w}{h_L} = 250\left(\dfrac{Re_{SG}}{Re_{SL}}\right)^{-5.07}X^{-5.48}$

between the two phases, which in turn causes pressure drop. By designing a piping system that can operate in a stratified flow, it can certainly increase safety and efficiency.

Several previous researchers (Govier and Omer (1962), Mandhane, et al. (1974),Taitel and Dukler (1976), Spedding and Nguyen (1979), Chen, et al. (1997), Fernandino and Ytrehus (2006) and Hudaya, et al. (2019)) has identified the interface structure of the stratified flow visually to describe the existing phenomena. In addition to using the visual method, Hudaya et al. (2019) identified the interface structure with image processing, where six sub-regimes of stratified flow were identified more clearly, namely: stratified smooth, 2D wave, 3D wave, roll wave, entrained droplet + disturbance wave and pseudo slug. Experimental studies on the interfacial wave characteristics of two-phase gas-liquid co-current flow in the horizontal pipe have been

carried out by several researchers using various methods. The signal processing method from the measurement of liquid film thickness was carried out by Mantilla et al. (2009) and Bae et al. (2017) using a parallel wire conductance probe, Al-Sarkhi et al. (2012) used a flush mounted conductance probe and Gawas et al. (2014) used a two-wire capacitance probe. Setyawan and Indarto (2016) used the constant electric current method (CECM) to measure liquid holdup. Meanwhile, Hudaya et al. (2019) using the image processing method from the results of image recording using a Highspeed Video Camera. The experimental conditions, measurement methods and the resulting equations can be seen in Table 1. Although the experimental study conducted by Bae et al. (2017) and Hudaya et al. (2019) have produced equations to predict wave parameters in stratified flow, but these equations have only been tested for air and water working fluids. Experimental studies with variations in the
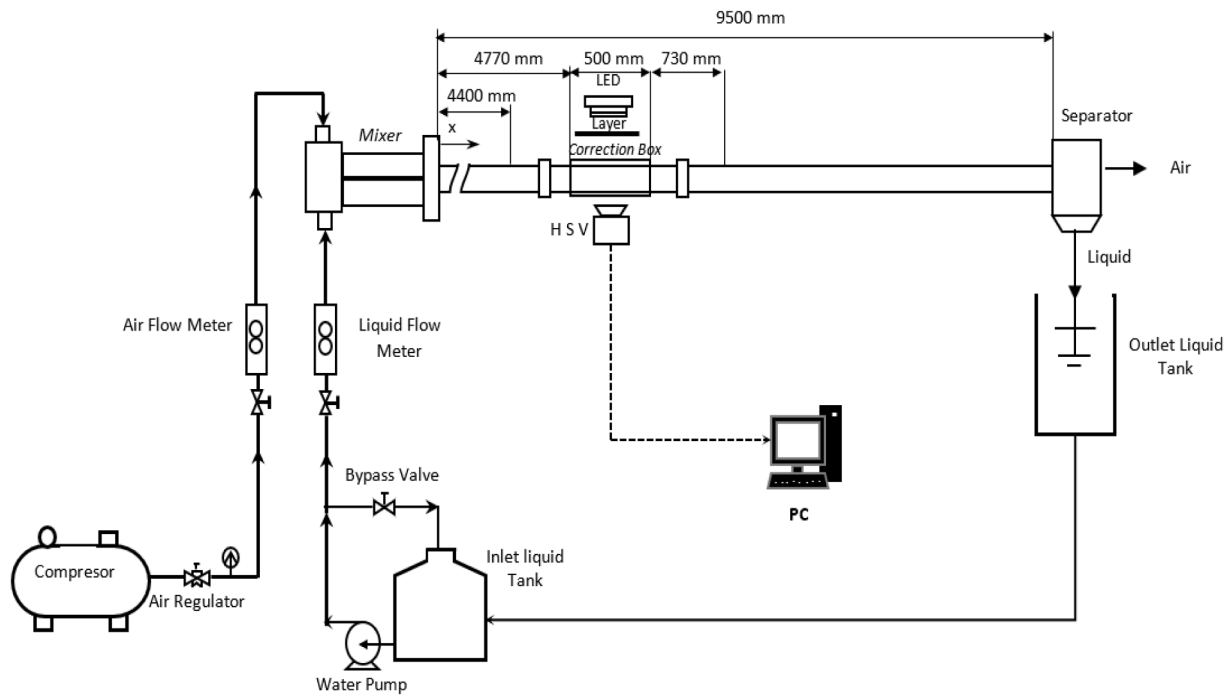
Fig. 1. Experimental apparatus.

physical properties of fluids need to be carried out to test and develop the previously generated correlations.

The effect of the physical properties of the liquid (viscosity and surface tension) on the wave parameters of the co-current gas-liquid two-phase flow in a horizontal pipe has been carried out by Mantilla et al. (2009) and Setyawan and Indarto (2016) on different regimes and experimental conditions. Mantilla et al. (2009) conducted a study on the stratified-annular regime with pipe inner diameters of 50.8 and 152.4 mm, while Setyawan and Indaro (2016) in the annular regime with pipe inner diameters of 16 and 26 mm. Experimental conditions, measurement methods and the resulting equations can be seen in Table 1. To complete the data base and obtain more comprehensive research results, the study of Mantilla, et al. (2009) need to be developed with a smaller pipe diameter, while the research of Setyawan and Indarto (2016) needs to be developed in a stratified regime.

The aim of the present experimental study is to investigate the effect of viscosity and surface tension of the liquid on the wave parameters (frequency and velocity) of gas-liquid stratified flow in horizontal pipe. Here, the developed image processing methods are used to obtain the quantitative parameters from the stratified flow data. Furthermore, a comprehensive analysis was carried out and compared with the previous studies' results. The dimensions analysis and fitting process of the present and previous researcher's data (Mantilla, et al., 2009, Setyawan and Indarto, 2016, Bae, et al., 2017) and Hudaya, et al., 2019) were applied to obtain the wave parameters correlation.

2. Experimental apparatus and method

Fig. 1 shows the schematic diagram of the experimental apparatus used in the present study. Air and water at atmospheric pressure were used as tested fluids. To vary the liquid viscosity, water was mixed with glycerin. The percentages of glycerin in the mixture were 30 and 50%. Meanwhile, to vary the surface tension of the liquid, water was mixed with butanol. The percentages of butanol in the mixture were 2 and 5%. To simplify the explanation in this paper, an abbreviation is used for the tested fluid based on the viscosity and surface tension of the liquid, namely **W**: air-water (*dynamic viscosity,* $\mu = 1.002$ mPa.s), **G30**: air-30 wt.% glycerin ($\mu = 2.773$ mPa.s), **G50**: air-50 wt.% glycerin ($\mu =$
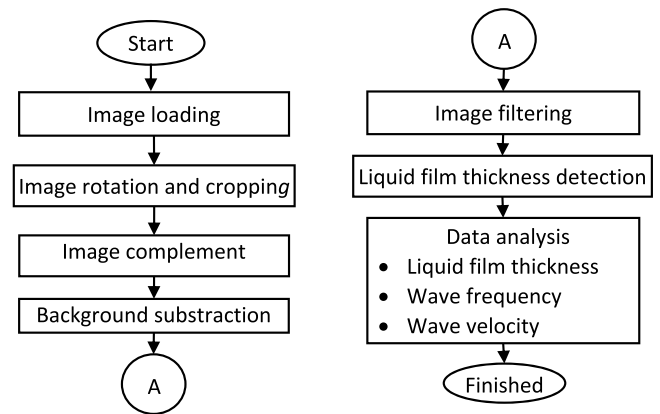

Fig. 2. The image processing steps.

6.292 mPa.s), **B2**: air-2 wt.% butanol ($\sigma = 58$ mN/m) dan **B5**: air-5 wt.% butanol ($\sigma = 42.5$ mN/m). The detail of the apparatus and method were described clearly by our former reports such as Hudaya et al. (2019), Catrawedarma and Deendarlianto (2021), and Wijayanta et al. (2022)

2.1. Image processing techniques

In general, the sequential steps of image processing used in the present work can be seen in Fig. 2. After the stratified flow phenomenon was recorded and transferred to a personal computer (**PC**) via Phantom Control Camera software, then the recorded video was extracted into a sequential grayscale image and loaded in Matlab for further processing. Although during the experiment the camera placement was adjusted with precision and care, but misadjustment between the horizontal axis between the pipe and the image still occurred and needed to be rotated. In addition, the cropping process was used to remove parts that were not used. The next step is the reversal of the image (image complement), which is the reversal of the value of each pixel which is replaced with a new value resulting from the subtraction of the maximum value (255) with its pixel value. The next step is background subtraction, which is
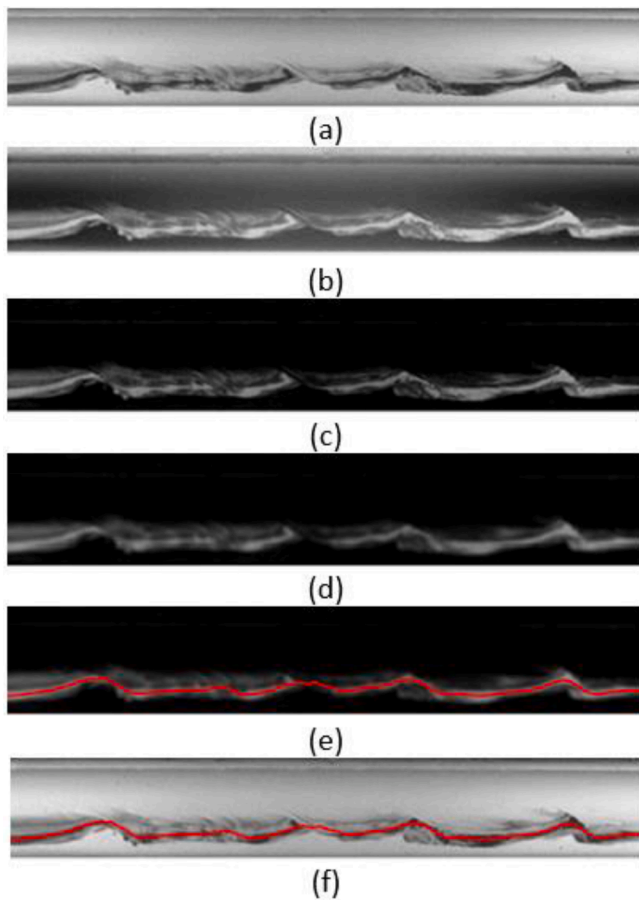
Fig. 3. (a) The raw image, (b) Complement process results, (c) Background subtraction process results, (d) Filtering process results, (e) The detection process of liquid film thickness, (f) The detection results of liquid film thickness in the grayscale image.

the process of reducing the image by reducing the complement image with a background image that has been complemented by the complement process. In this study, a grayscale background image was created by combining a full air background image and a full water background image (top area: full air; bottom area: full water). This combination method has previously been carried out by Kuntoro et al. (2016) and

Hudaya et al. (2019). Next, a filtering process is used to remove noise. Next, the liquid film thickness was detected, where the principle is to detect the position of the maximum gray value in each pixel column in the image. Liquid film thickness data was measured by calculating the distance between the y-coordinate of the base position and the position of the maximum gray value. Furthermore, the results of the detection of the liquid film thickness were plotted into a gray scale image. The results of the image processing process can be seen in Fig. 3.

In addition, a smoothing process was carried out to overcome local blindness in the liquid film thickness detection process. Fig. 4 shows that the edge detection process cannot be optimal because the interface was blurry, so the results show a fluctuating interface. A smoothing process was carried out to overcome this problem. Furthermore, the edge detection results were plotted, where the stratified interface was well displayed. As shown in Fig. 4(c), the result of the liquid film thickness detection from image processing is in pixels. To convert from the pixels into the mm, it is calculated by multiplying the result of the liquid film thickness detection in pixels by the ratio of mm per pixel (mm/pixel). The inside diameter of the pipe (26 mm) which clearly shows the upper and lower limits on the raw image is used as a reference to be converted to pixel units using Phantom Camera Control (PCC) Application software. From the conversion results, the value of the inside diameter of the pipe (26 mm) is equal to 82 pixels, so the ratio of mm per pixel is 0.32. This number is the smallest unit value of this measurement. Absolute uncertainty is equal to half of the smallest unit value, which is $0.5 \times 0.32 = 0.16$. Thus, the uncertainty of the results of measuring the liquid film thickness in this study is ± 0.16 mm.

2.2. The measurement of the wave parameter

The method of measuring liquid film thickness, wave frequency, and wave velocity was the same as that carried out by Hudaya et al. (2019) as follows:

a The thickness of the liquid film

The liquid film thickness data extraction was carried out at four different reference locations as shown in Fig. 5(a). The sequential steps of image processing were carried out for all recorded data to obtain liquid film thickness data as a function of time. Each reference location produces liquid film thickness data as a function of time as shown in Fig. 5(b).
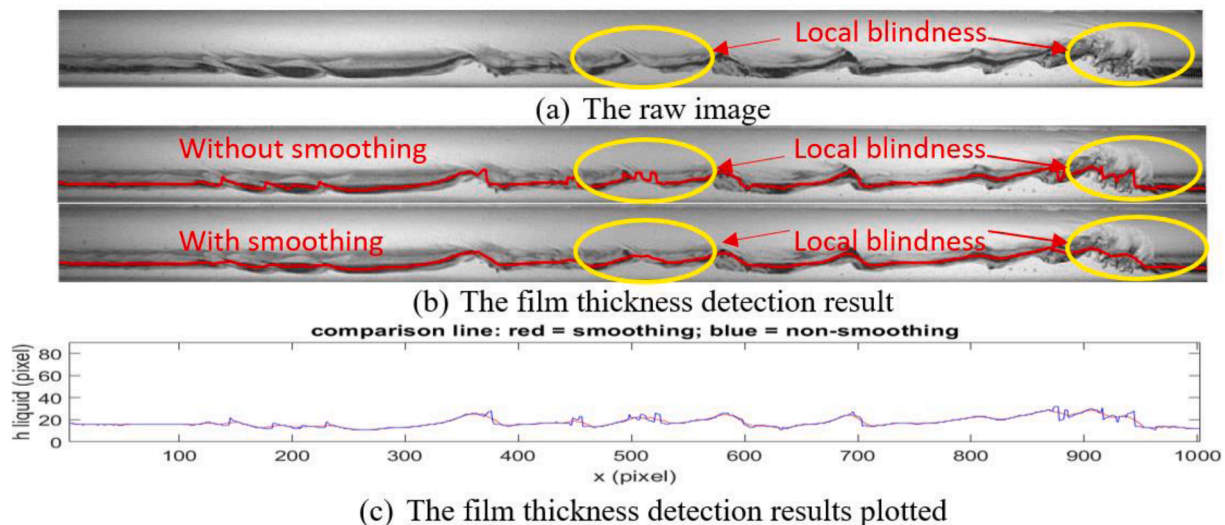
a The wave frequency

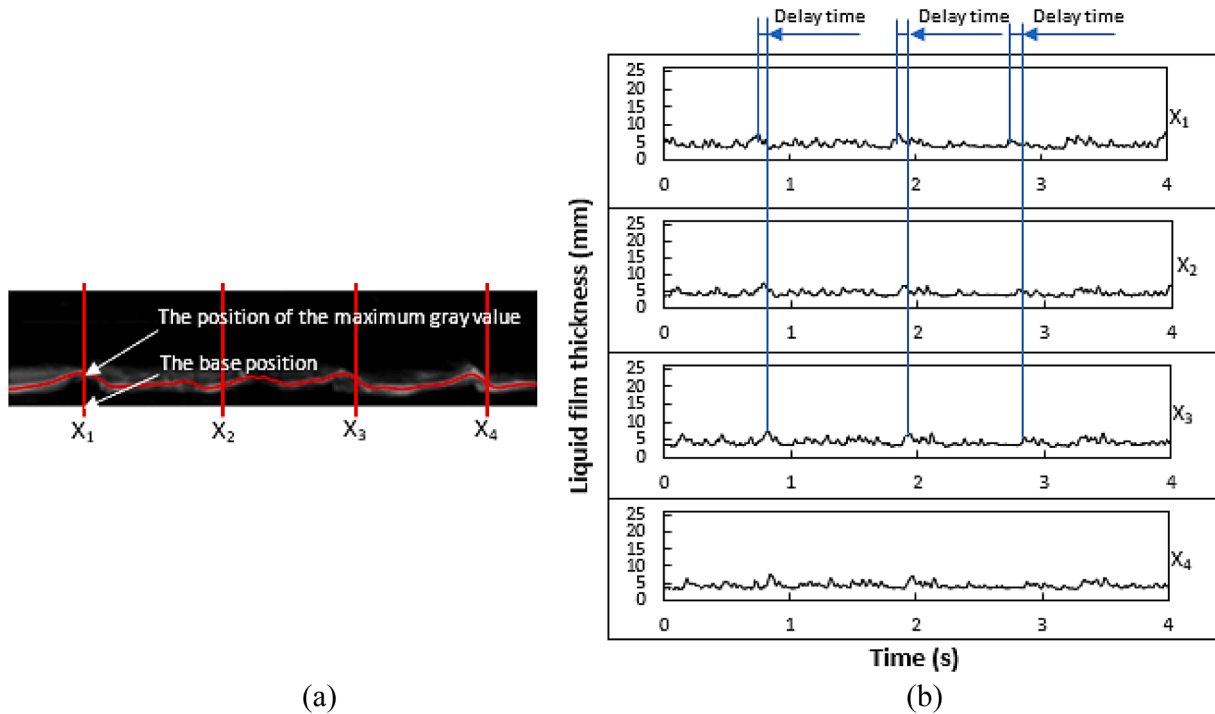**Fig. 4.** The local blindness smoothing process on the film thickness detection.

Fig. 5. (a) Detection results of liquid film thickness (b) the time series plot of liquid film thickness.
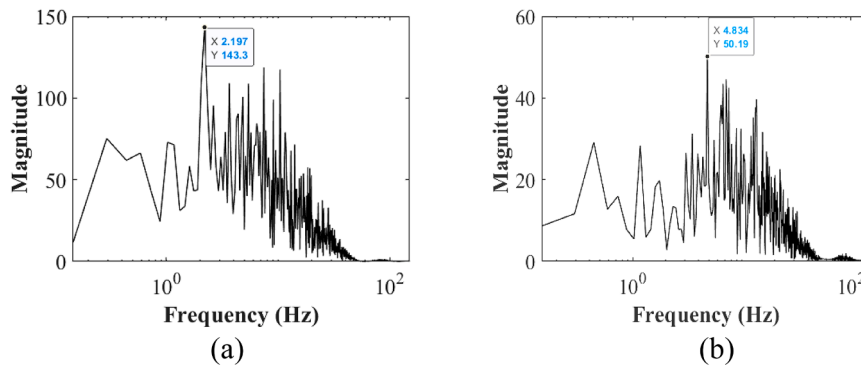

Fig. 6. Determination of wave frequency with power spectral density (PSD) at J_L= 0.03 m/s with J_G = (a) 10 m/s and (b) 14 m/s with tested liquid **W**.

The liquid film thickness data resulting from image processing which is the time domain was analyzed into the frequency domain using the Power Spectral Density (PSD) function. The frequency of the interface wave was determined based on the value of the dominant frequency which has the largest magnitude value as shown in Fig. 6.

a The wave velocity

By using cross-correlation, the time delay between signals can be calculated. Cross-correlation $R_{xy}(t)$ of the signals x(t) and y(t) is defined as:

$$R_{xy}(t) = \int_{-\infty}^{\infty} x(\tau)y(t+\tau)d\tau \qquad (1)$$

The delay time (t), corresponds to the maximum value of the cross-correlation function $R_{xy}(t)$. For example, as can be seen in Fig. 5, this time delay is the average time of the wave to propagate from reference location 1 (x1) to reference location 2 (x3). By knowing the distance between the two locations, the wave velocity can be determined.

3. Result and discussion

3.1. The stratified flow sub-regime maps

In the present experimental study, the criteria for dividing the interface waves refers to the proposed criteria by several previous researchers (Chen, et al., 1997; Hudaya et al., 2019; Wijayanta, et al., 2022) as follows:

(a) Two-dimensional (2-D) wave flow. Here, the interface is basically flat without any crosswise curvature at the interface.

(b) Three-dimensional (3-D) wave flow. Some parts of the liquid phase tend to climb the inner wall of the pipe due to the wave spreading effect, and there is a slight/crosswise curvature at the interface close to the pipe wall.

(c) Roll wave (RW) flow. Here, some parts of the liquid phase rise up the inner wall of the pipe and a significant concave down curvature is formed at the air-water interface.

(d) Entrained droplet + Disturbance wave (ED + DW) flow. Some parts of the liquid droplets escape from the liquid surface and entrainment/deposition phenomena occur. As the superficial

(a) **W** (Wijayanta, et al., 2002)

(b) **G30** (Wijayanta, et al., 2002)

(c) **G50** (Wijayanta, et al., 2002)

(d) **B2**

(e) **B5**
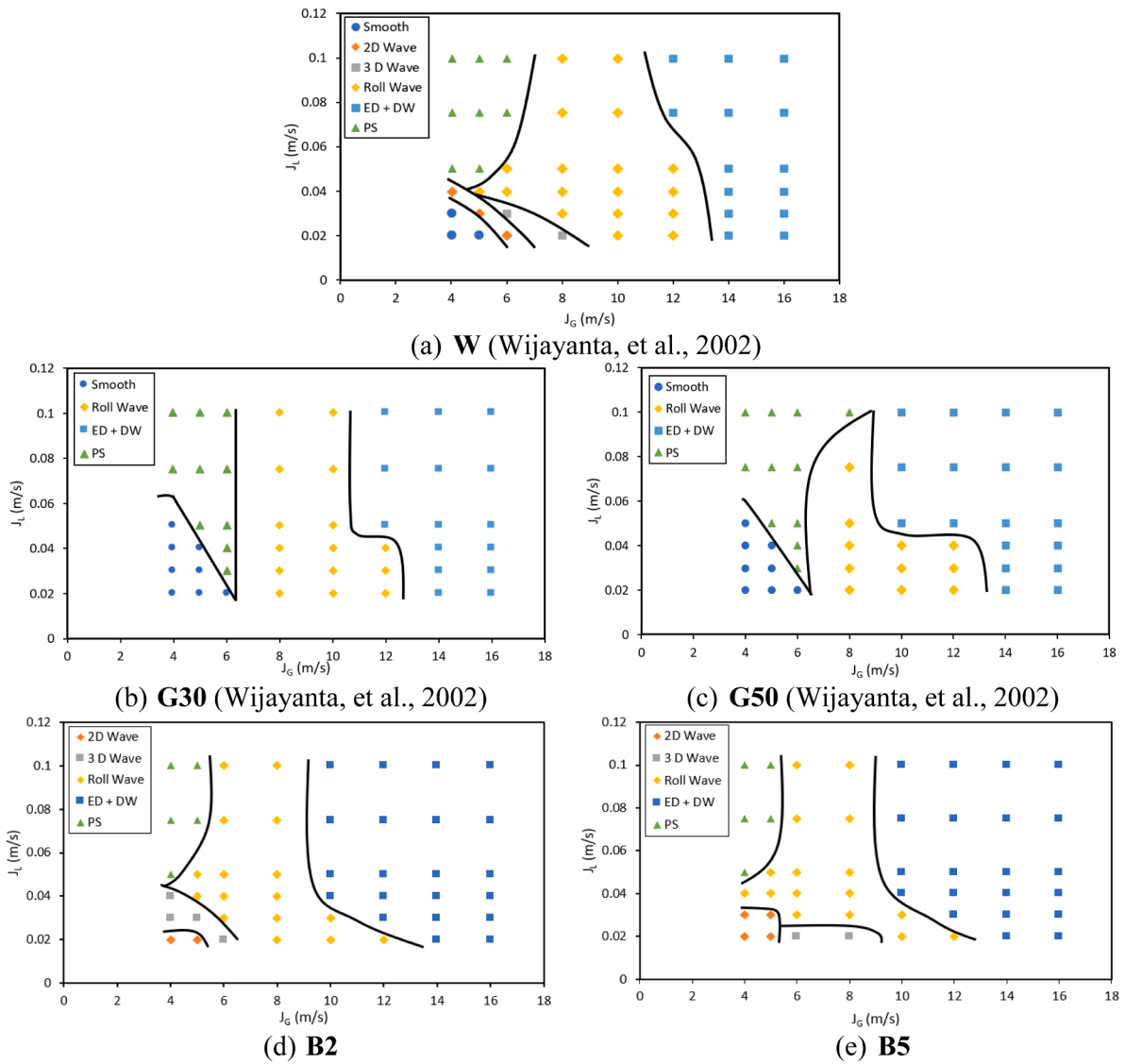
Fig. 7. Sub-regime map on gas-liquid stratified flow with five variations of the tested liquid

velocity of the gas increases, a significant fraction of the entrainment of the liquid appears in the air stream. It is estimated that an annular flow pattern occurs if the superficial gas velocity is high enough.

(e) Pseudo slug (PS). This sub-regime is characterized by a sudden increase in waves (hydraulic jump) until it reaches the top of the pipe, but the liquid has not completely filled the cross section of the pipe and is immediately decayed by the force of the air. This event is called as the pseudo slug, because there is no blockage in the pipe.

In the present experimental study, with the working fluid **W**, the sub-regimes identified in the stratified flow based on the interfacial wave structure were the same as those identified by Hudaya et al (2019) and Wijayanta et al (2022). Those are stratified smooth (S), two-dimensional (2-D) wave, three-dimensional (3-D) wave, roll wave (RW), pseudo slug (PS), and entrained droplet + disturbance wave (ED + DW) as can be seen in Fig. 7. In the experiment of the tested liquid of **G30** and **G50**, 2-D and 3-D wave did not appear during the observation. In the experiment with the tested liquid of **B2** and **B5**, stratified smooth did not appear during the observations.

Sub-regime maps of gas-liquid stratified flow with three variations of

the test fluids **W, G30**, and **G50** have been carried out by Wijayanta et al (2022) as shown in Fig. 7(a–c). From the figure, it is noticed that as the viscosity of the liquid increases, the transition lines (J_L and J_G) from RW to ED + DW shift downward. The increase of the liquid viscosity will decrease the RW region, while the S, PS, and ED + DW regions increase, which is in accordance with the research results of Matsubara and Naito (2011). Meanwhile, from Fig. 7(a,d,e), it can be seen that the decrease in the liquid surface tension from **W** to **B2** and **B3** causes the transition lines (J_L and J_G) from RW to ED + DW to shift downwards. The decrease of the liquid surface tension will decrease the PS region, eliminating the stratified smooth region, and increasing the 3-D wave region for **B2** and the 2D wave region for **B5**. Fig. 8 shows an example of the physical mechanism of the transition or formation of each stratified flow sub-regime, while a more detailed discussion can be seen in Wijayanta et al. (2022).

In the present experimental study, the interface structure for the stratified smooth (S), roll wave (RW) and entrained droplet + disturbance wave (ED+DW) sub regimes can be captured by a highspeed video camera from a side view in the direction of the flow clearly according to the criteria. Moreover, to get a clear picture of the interface structure criteria of the 2-D wave and 3-D wave sub-regimes, a highspeed video camera was recorded from the side and top views in the direction of the
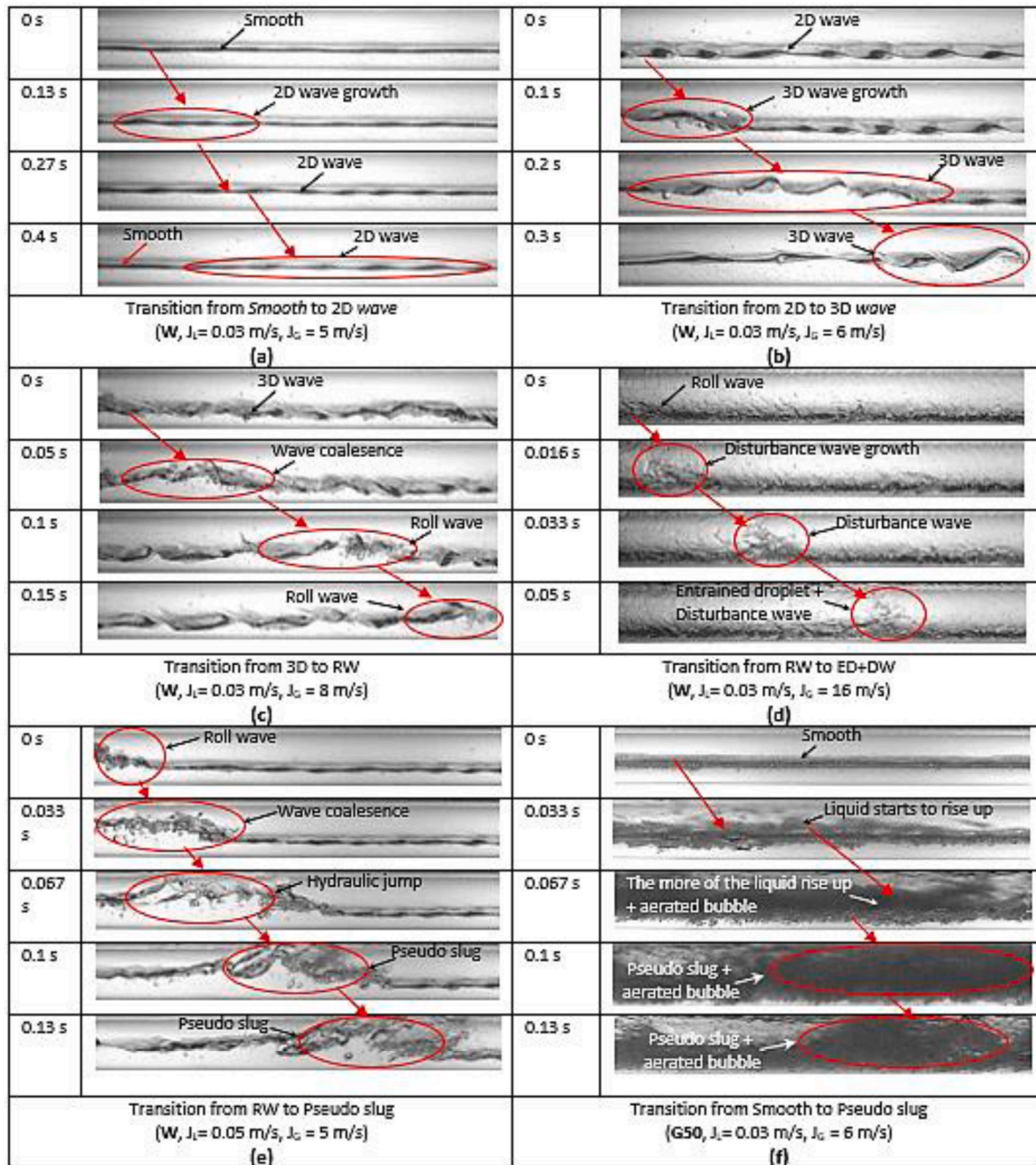
Fig. 8. The physical mechanism of gas-liquid stratified flow sub-regime transition (Wijayanta, et al., 2022).

flow. Picture. shows an example of a top view of the interface structure of the 2-D wave and 3-D wave sub regimes. In Fig. 9(a), it can be seen that the addition of a small amount of J_G from the stratified smooth sub-regime conditions causes the growth of 2-D waves. It can be seen that some relatively uniform curved interface forms appear in the direction of the gas and liquid flow. There is no visible interface curvature in the direction crosswise of flow. This is in accordance with the criteria of 2-D waves. In Fig. 9(b), it can be seen that the addition of J_G from the condition of the 2-D wave sub regime causes instability at the periphery near the inner side of the pipe. This causes a wave to grow near the right side of the inside of the pipe and hit the right side of the inside of the pipe. The thrust of the gas flow against the wave will form an interfacial curvature in the direction of the fluid flow, while from the right wall the inside of the pipe provides a back thrust to the left across the flow. As a result, the curvature of the interface will be greater moving forward in

the direction of the flow and to the left across the flow until it hits the left side wall of the pipe. This causes the inner left wall of the pipe to provide a back thrust towards the right across the flow. The meeting of the thrust from the right and left side walls of the pipe causes the resultant force to be zero and the interfacial curvature is lost from the crosswise direction of flow. The thrust and movement of this 3D wave formation also affects the movement and curvature of the wave interface in front of it, so that both waves lose the interface curvature (straight across the flow). Next, the gas flow pushes the two waves so that they merge and move forward in the direction of the fluid flow as per the 2D wave criteria.

3.2. Stratified flow interfacial wave parameters

3.2.1. Liquid film thickness

The examples of the interfacial behavior, time-series, probability
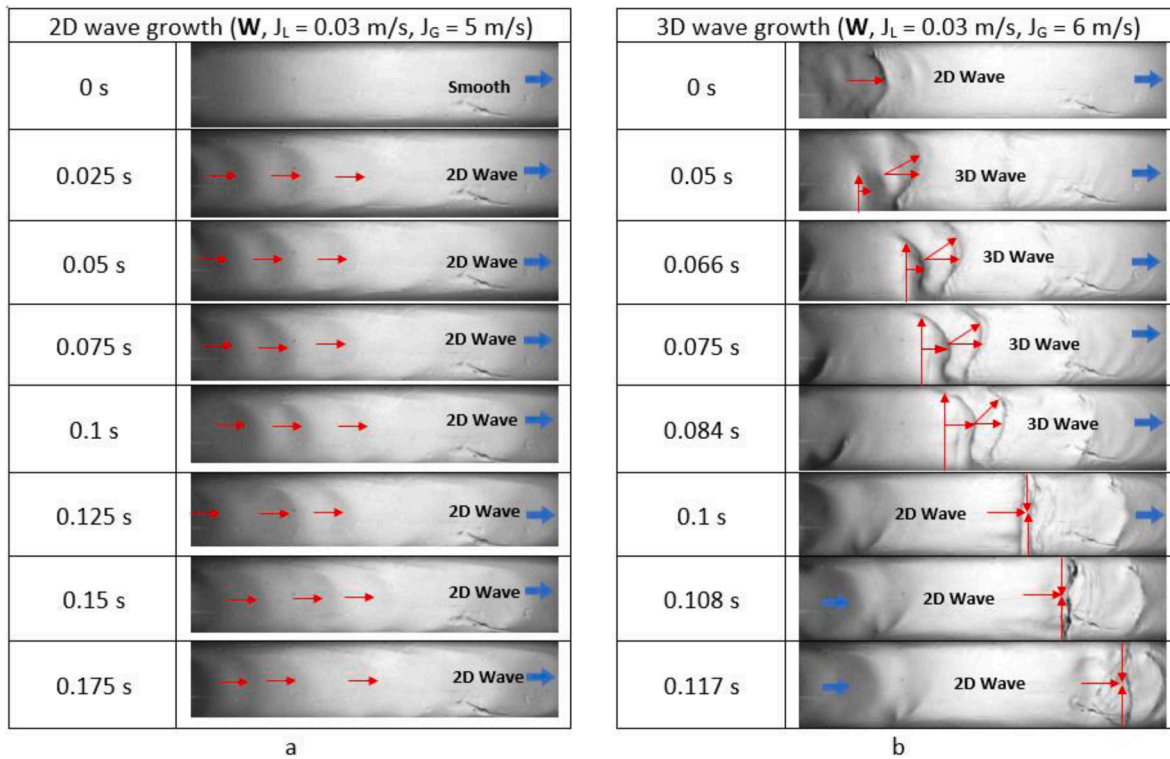
Fig. 9. Example of a top view of the interface structure of the 2-D wave and 3-D wave sub regimes

distribution function (PDF), and wavelet transform of the liquid film thickness (h_L) of each stratified flow sub-regime under the variations of viscosity and surface tension can be seen in Tables 2–6. The use of wavelet transforms of the liquid film thickness data to identify the stratified flow sub-regimes is in principle the same as of Wijayanta et al. (2022) using pressure gradient signals. As reported by Elperin and Klochko (2002), the wavelet transform can provide a time scale for signal decomposition as an intermediary between the time and frequency domains. In the decomposed signal, the frequency band decreases with the increase of the signal scale. Catrawedarma and Deendarlianto (2021) reported that level one detail (D1) shows the largest frequency band with the smallest scale, while D2, D3, and so on show a larger scale with a lower frequency. The basic theory and discrete wavelet transform (DWT) algorithm have been described in detail by Mallat (1989).

From the example of experimental results using the tested liquid of **W** (Table 2), it can be seen that in the small 2-D wave sub-regime, relatively uniform small waves appear. From the time series of the liquid film thickness, it can be seen that the fluctuation of liquid film thickness (h_L) is small. From the PDF, it can be seen that the distribution of the data appears to be clustered at h_L of approximately 5 ± 0.16 mm to 6 ± 0.16 mm. In addition, from the wavelet transform, the largest wavelet energies are found in D5 and D8. Large-scale and low-frequency detail (D8) in the fluctuations of liquid film thickness was caused by the appearance of clustered and intermittent small 2D waves. Meanwhile, inside the 2-D wave clusters, small 2-D waves were formed with fluctuations in the liquid film thickness which are much smaller than the 2-D wave clusters as indicated by the medium detail of scale and frequency (D5). From the experimental results using the tested liquid of **G30** (Table 3) and **G50** (Table 4), there is no visible both 2-D and 3-D waves. Meanwhile, from the experimental results using the tested liquid of **B2** (Table 5) and **B5** (Table 6), small 2-D waves were formed at J_L and J_G which were lower than the experiment with the tested liquid of **W**. The fluctuations of liquid film thickness were smaller with a higher frequency in comparison to that of the height of the formed small 2-D waves in the experiment

using the tested liquid of **W**. From the time-series of the liquid film thickness, it can be seen that the fluctuation of liquid film thickness (h_L) was small. From the PDF, it can be seen that the distribution of the data appears to be clustered at h_L of approximately 5 ± 0.16 mm. In addition, from the wavelet transform, the largest wavelet energy in the detail of the scale and frequency of medium (D5), which shows fluctuations in the liquid film thickness, and the frequency of small 2- D waves were medium size.

From the experimental results using the tested liquid of **W** (Table 2), the increase of the superficial gas velocity from the 2-D wave condition causes a change in shape to a 3-D wave. The waveform looks irregular in the lateral direction. From the time series of the liquid film thickness, it can be seen that the fluctuation of the liquid film thickness is higher than that of the small 2-D wave. From the PDF, the distribution of liquid film thickness spreads from about 4 ± 0.16 mm to 9 ± 0.16 mm. In addition, from the wavelet transform, the largest wavelet energy is located in the large-scale detail and low frequency (D9). This means that the fluctuation of liquid film thickness is in large scale with low frequency. Meanwhile, from the experimental results using the tested liquid of **B2** (Table 5), it can be seen that the formed 3-D wave is longer than that of **W**. From the time series of the liquid film thickness and the PDF, it is noticed that the distribution of the liquid film thickness data is spread from about 4 ± 0.16 mm to 11 ± 0.16 mm. From the wavelet transform, the largest wavelet e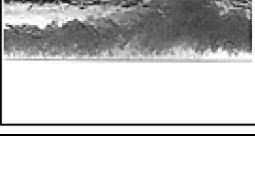nergy is located at D9 equal to the tested liquid **W**. From the experimental results using the tested liquid of **B5** (Table 6), visually it can be seen that the formed 3-D wave is shorter than the experiment using the tested liquid of **W** and **B2**. From the time series of liquid film thickness and PDF, it shows the distribution of liquid film thickness data spreads from about 3 ± 0.16 mm to 6 ± 0.16 mm. From the wavelet transform, the largest wavelet energy is also located at D9.
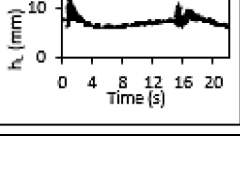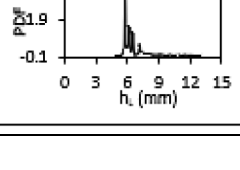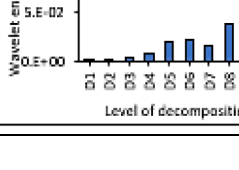
From the experimental results using the tested liquid of **G30** (Table 3) and **G50** (Table 4) under the flow condition of $J_L = 0.03$ m/s, the increase of J_G from the stratified smooth condition causes a hydraulic jump. This was defined by Lin and Hanratty (1987) as a characteristic of the pseudo slug. In addition, the decrease of J_G (5 m/s) at

Table 2

Example of photograph, time series, PDF and Wavelet energy of the liquid film thickness with the tested liquid of **W**

No	Sub Rezim, J_L & J_G	Foto (a)	The time series plot (b)	PDF (c)	Wavelet energy (d)
i	Small 2D Wave $J_L = 0{,}03$ m/s $J_G = 5$ m/s				
ii	Large 3D Wave $J_L = 0{,}03$ m/s $J_G = 6$ m/s				
iii	Medium Roll Wave $J_L = 0{,}03$ m/s $J_G = 8$ m/s				
iv	Small Roll Wave $J_L = 0{,}03$ m/s $J_G = 10$ m/s				
v	ED + DW $J_L = 0{,}03$ m/s $J_{G} = 16$ m/s				
vi	Pseudo Slug $J_L = 0{,}05$ m/s $J_G = 5$ m/s				

higher J_L (0.05 m/s) causes the hydraulic jump to be larger. This also happened in the experiment using the tested liquid of **W**. Meanwhile, from the experimental results using the tested liquid of **B2** (Table 5) and **B5** (Table 6) with the same J_L (0.05 m/s), the hydraulic jump occurred at the J_G which was lower again (4 m/s). This is in accordance with what was stated by Dukler and Hubbard (1975) as a transition from stratified to intermittent. From the liquid film thickness time-series, the fluctuation of the liquid film thickness signal is seen to be the largest compared to the other sub-regimes. From the PDF, it forms a long tail as a characteristic of the pseudo slug sub-regime. From the wavelet transform, the largest wavelet energy is located in D9 and D10 with the largest wavelet energy value compared to other sub-regimes.
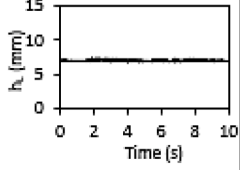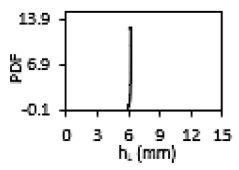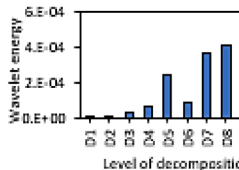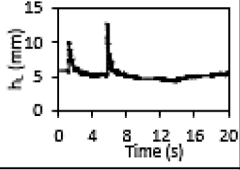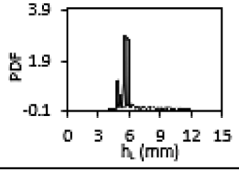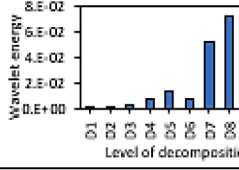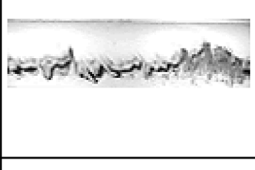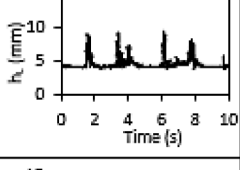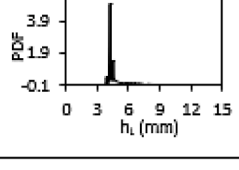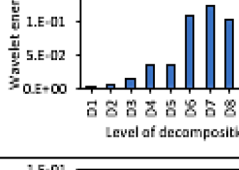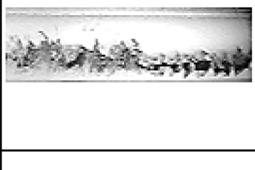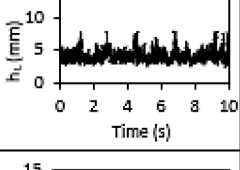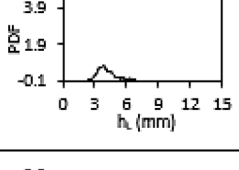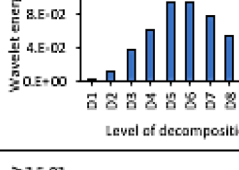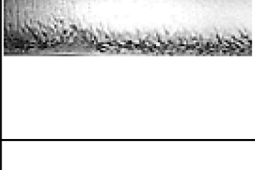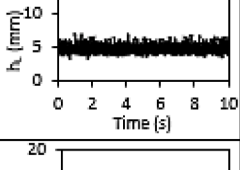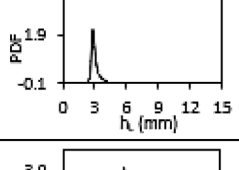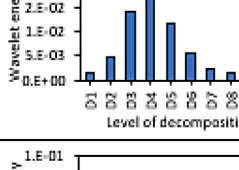
From the experimental results using the tested liquid of **W** (Table 2), **G30** (Table 3) and **G50** (Table 4) under the flow condition of $J_G = 8$ m/s, a medium-sized RW sub-regime was formed, and at $J_G = 10$ m/s, a small-sized RW sub-regime was formed. From the time series and PDF, the fluctuation of the liquid film thickness signals on medium RW also look larger than that of small RW. From the wavelet transform for the tested liquid of **W** (Table 2), the largest wavelet energy for the medium RW was

located at D6, while for the small RW it was at D5. This shows that the increase of J_G causes the RW frequency formed to be higher, but the scale or size was getting smaller. Meanwhile, from the wavelet transform for the tested liquid of **G30** (Table 3) and **G50** (Table 4), the largest wavelet energy for the medium RW was located at D7. The largest wavelet energy of the small RW for the **G30** was located on D5, while for the **G50**, it was located on D4. It shows that the increase of the viscosity of the liquid causes the wavelet energy to shift slightly to a larger scale, but with a lower frequency.

From the results of the experiment using the tested liquid of **B2** (Table 5) and **B5** (Table 6) under the flow condition of $J_G = 6$ m/s, a large RW was formed. The height of the wave was almost the same as the large 3-D wave, but it rolls. From the time series, it can be seen that the fluctuation of liquid film thickness was also almost the same as that of large 3-D waves. From the PDF, it has a long tail like the large 3-D wave and PS. Meanwhile, from the wavelet transform, the largest wavelet energy for **B2** was located at D9, while for **B5** it was located at D7. At $J_G = 8$ m/s, medium RW occurs, while at $J_G = 10$ m/s, small RW occurs. In the medium RW, the largest wavelet energy for **B2** and **B5** were located

Table 3

Example of photograph, time series, PDF and Wavelet energy of the liquid film thickness with the tested liquid of **G30.**

No	Sub Regime, J_L & J_G	Photograph (a)	The time series plot (b)	PDF (c)	Wavelet energy (d)
i	Smooth J_L = 0.03 m/s J_G= 5 m/s				
ii	Pseudo Slug J_L = 0.03 m/s J_G= 6 m/s				
iii	Medium Roll Wave J_L = 0.03 m/s J_G= 8 m/s				
iv	Small Roll Wave J_L = 0.03 J_G= 10				
v	ED + DW J_L = 0.03 m/s J_G= 16 m/s				
vi	Pseudo Slug J_L = 0.05 m/s J_G= 5 m/s				

on D5. In small RW, the largest wavelet energy for **B2** was located at D6, while for **B5** it was located at D5, the same as for the tested liquid of **W**. From the wavelet energy, it shows that the decrease of the surface tension has no effect on the shift in scale and frequency of the largest wavelet energy.
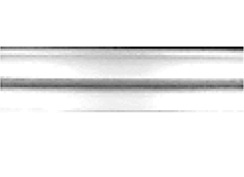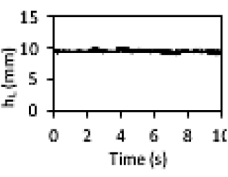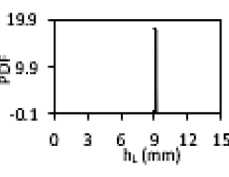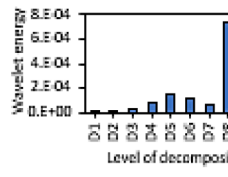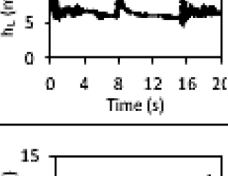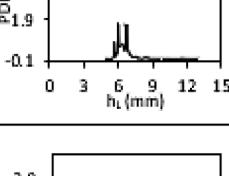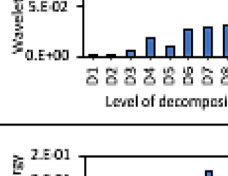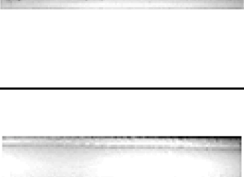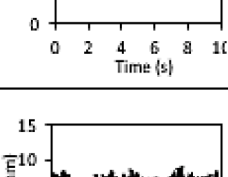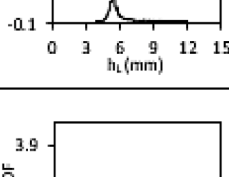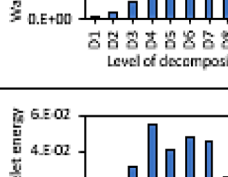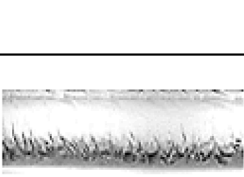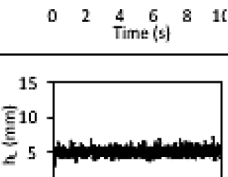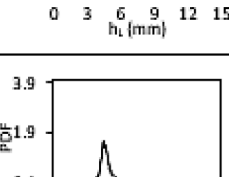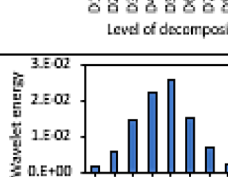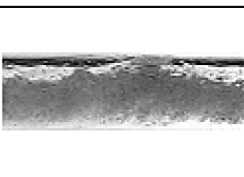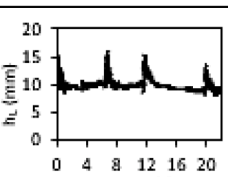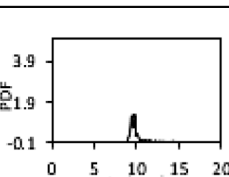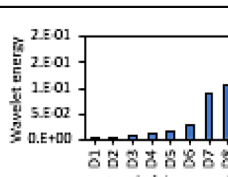
From the results of the experiment using the tested liquids of **W, G30, G50, B2,** and **B5,** under the J_G = 14 m/s and 16 m/s the sub-regime ED + DW was formed. From the time series and PDF 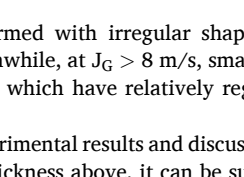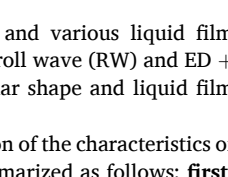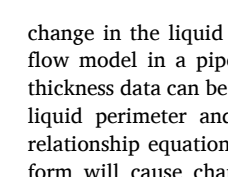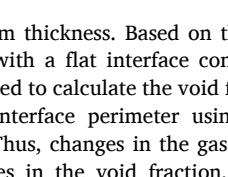for the **W, G30, G50**, the distribution of liquid film thickness looks more uniform than the 3-D wave, RW and PS. Meanwhile, from the wavelet transform, the largest wavelet energy for **W** and **G30** was located on D4, while for **G50** it was located on D5. This shows that the increase of the viscosity of the liquid causes the scale of the fluctuation of the liquids film thickness to be larger, but the frequency was lower. For the tested liquid of **B2** and **B5**, more liquids were lifted up to form droplets and some sticks to the top and sides of the inner wall of the pipe. The time series looks flatter than **W, G30** and **G50**. This shows that the decrease of the surface tension of the liquid causes the liquid to be more easily lifted and become droplets, hence the liquid film thickness becomes flatter and

uniform. From the PDF, it can also be seen that the distribution of liquid film thickness was more uniform than that of 3-D wave, RW and PS. Meanwhile, from the wavelet transform, the largest wavelet energy was located at D4 the same as in the tested liquid of **W**. This shows that the decrease of the surface tension of the liquid does not affect the shift in scale and frequency of the wavelet energy.

The effect of the both viscosity and surface tension on the average liquid film thickness can be seen in Fig. 10, where variations in liquid viscosity have a large influence on the average liquid film thickness. The increase of the liquid viscosity causes an increase in the liquid film thickness. Meanwhile, the liquid surface tension variation has very little effect on the liquid film thickness. At J_G = 10 m/s, the average liquid film thickness tends to increase slightly with the decrease of the surface tension. Meanwhile, at J_G > 10 m/s, the decrease of surface tension has no effect on the average liquid film thickness. This is because most of the liquid is lifted up to form droplets and some sticks to the top and sides of the inner wall of the pipe. From Fig. 10, it can be seen that at $J_G \leq$ 8 m/s, the error bar of the average liquid film thickness on the graph is larger than at J_G > 8 m/s. This is because at $J_G \leq$ 8 m/s, 3-D waves and Pseudo

Table 4

Example of photograph, time series, PDF and Wavelet energy of the liquid film thickness with the tested liquid of **G50.**
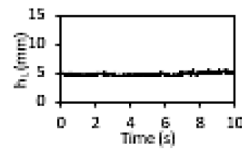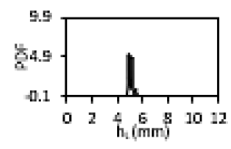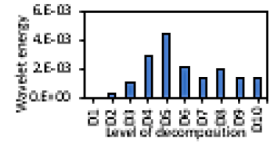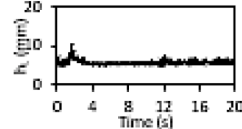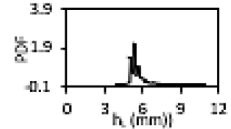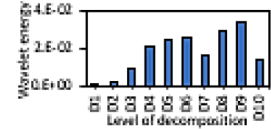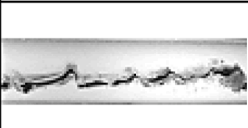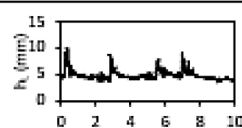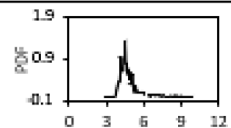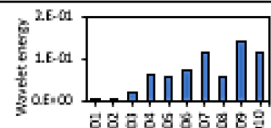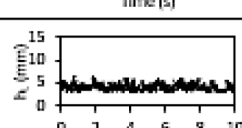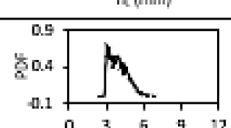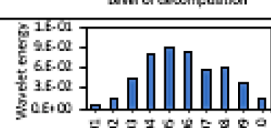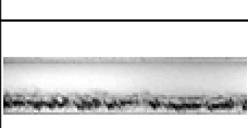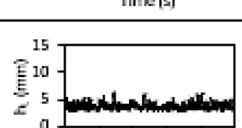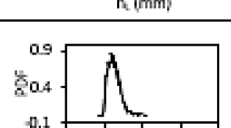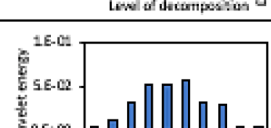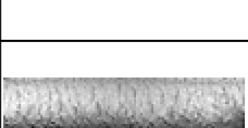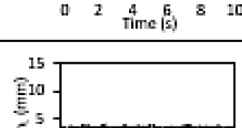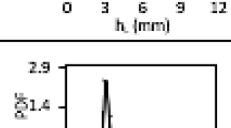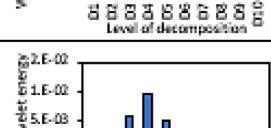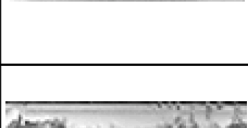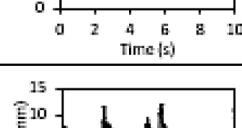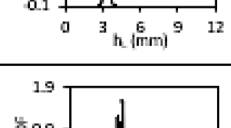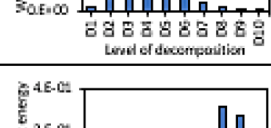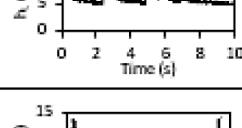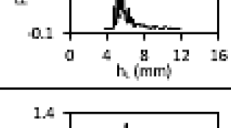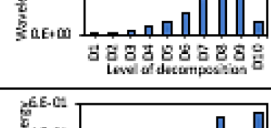
No	Sub Regime, J_L & J_G	Photograph (a)	The time series plot (b)	PDF (c)	Wavelet energy (d)
i	**Smooth** J_L = 0.03 m/s J_G = 5 m/s				
ii	**Pseudo Slug** J_L = 0.03 m/s J_G = 6 m/s				
iii	**Medium Roll Wave** J_L = 0.03 m/s J_G = 8 m/s				
iv	**Small Roll wave** J_L = 0.03 m/s J_G = 10 m/s				
v	**ED + DW** J_L = 0.03 m/s J_G = 16 m/s				
vi	**Pseudo Slug** J_L = 0.05 m/s J_G = 5 m/s				

Slug (PS) are formed with irregular shapes and various liquid film thicknesses. Meanwhile, at J_G > 8 m/s, small roll wave (RW) and ED + DW were formed which have relatively regular shape and liquid film thickness.

From the experimental results and discussion of the characteristics of the liquid film thickness above, it can be summarized as follows: **first**, the gas-liquid interface waveform of each stratified flow sub regime can be identified from the results of liquid film thickness detection using image processing. **Second**, the superficial gas velocity (J_G) greatly influences the liquid film thickness, where an increase in J_G causes the liquid film thickness to decrease. **Third**, variations in liquid viscosity have a large influence on the average liquid film thickness. The increase of the liquid viscosity causes an increase in the liquid film thickness. Meanwhile, the liquid surface tension variation has very little effect on the liquid film thickness. If we study further from the **first** point, the change of the gas-liquid interface waveform will be followed by a change in the liquid film thickness. Based on the stratified gas-liquid flow model in a pipe with a flat interface configuration, liquid film thickness data can be used to calculate the void fraction, gas perimeter, liquid perimeter and interface perimeter using the pipe geometric relationship equation. Thus, changes in the gas-liquid interface waveform will cause changes in the void fraction, gas perimeter, liquid perimeter and interface perimeter. Based on the momentum conservation equation, changes in the void fraction, gas perimeter, liquid perimeter and interface perimeter will have an impact on changes in interfacial shear stress and pressure gradient. Thus, based on the **second** and **third** points above, J_G, liquid viscosity and liquid surface tension are important parameters in developing correlations to predict void fraction, interfacial shear stress and pressure gradient as future research work.

Table 5

Example of photograph, time series, PDF and Wavelet energy of the liquid film thickness with the tested liquid of **B2.**

4. The wave frequency

The effect of J_G on wave frequency under the variation of J_L with the tested liquid of **W, G30, G50, B2,** and **B5** is shown in Table 7. At $J_G = 8$ m/s the relationship between J_G and frequency for almost all J_L variations and the tested liquid has a complex tendency. This is caused by the appearance of the 2-D wave, 3-D wave, and PS with various shapes and time lag with low frequency. In Table 7 it can be seen that from the entire J_L range in this experiment, at $J_G > 8$ m/s, the frequency of the wave tends to increase with J_G. This is due to the increased slip between the air and liquid velocities, so that the interfacial waves are more easily formed and their frequency increases. In the present experimental study, the RW and ED+DW sub-regimes are formed at the interface, where the frequency of the waves decreases with the increase in the viscosity of the

liquid. This is due to the increase of the stabilizing effect of increasing the viscosity of the liquid, so that more energy is required to form waves. This is in accordance with the results of Setyawan and Indarto (2016) who suggested that increasing the viscosity of the liquid causes a decrease in the wave frequency. Meanwhile, at $J_L \leq 0.04$ m/s and the $J_G \geq 10$ m/s, the addition of butanol or a decrease in the surface tension of the liquid causes an increase in the wave frequency. At $J_L > 0.04$ m/s and $J_G \geq 10$ m/s, the addition of butanol or a decrease in the surface tension causes the frequency of the wave decreases. This is in accordance with the results of Setyawan and Indarto (2016) which was conducted at $J_L = 0.05$ m/s to 0.2 m/s and $J_G = 12$ m/s to 40 m/s, which suggests that the wave frequency decreases with the decrease of the liquid surface tension for all ranges of experimental conditions.

Based on the discussion of Table 7 above, the emergence of 2-D wave,

Table 6

Example of photograph, time series, PDF and Wavelet energy of the liquid film thickness with the tested liquid of **B5.**
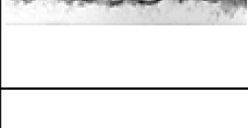
No	Sub Regime, J_L & J_G	Photograph (a)	The time series plot (b)	PDF (c)	Wavelet energy (d)
i	Small 2D Wave $J_L = 0.02$ $J_G = 4$				
ii	Small 3D Wave $J_L = 0.02$ $J_G = 6$				
iii	Large 2 D Wave $J_L = 0.03$ $J_G = 5$				
iv	Large Roll Wave $J_L = 0.03$ $J_G = 6$				
v	Small Roll Wave $J_L = 0.03$ $J_G = 8$				
vi	Small Roll wave $J_L = 0.03$ $J_G = 10$				
vii	Entrained Droplet + DW $J_L = 0.03$ $J_G = 16$				
viii	Large Roll Wave $J_L = 0.05$ $J_G = 5$				
ix	Pseudo Slug $J_L = 0.05$ $J_G = 4$				

3-D wave and PS produces a J_G relationship to the wave frequency for all J_L variations and the tested liquid was quite complex. Thus, the development of correlation to predict wave frequency will be focused on RW and ED + DW with $J_G > 8$ m/s. Several researchers have proposed the correlations for predicting the wave frequencies in gas-liquid two-phase flow as summarized in Table 1. However, correlations for predicting frequencies especially in stratified flow by experiments using variations in surface tension and viscosity of liquids have not been studied. The correlations proposed by the previous researchers used the nondimensional parameters X (modified Martinelli parameter) and St (Strouhal number):

$$St = \frac{fD}{J_L} \tag{2}$$

$$X = \sqrt{\frac{\rho_L}{\rho_G} \frac{J_L^2}{J_G^2}} \tag{3}$$

Fig. 11. shows the comparison of the wave frequency from the present experimental results and from previous researchers. From the Fig. 11, it is shown that the data from the present experiment have the same trend with that of previous works, whereas, the Strouhal number decreases with the increase of Martinelli parameter. The proposed
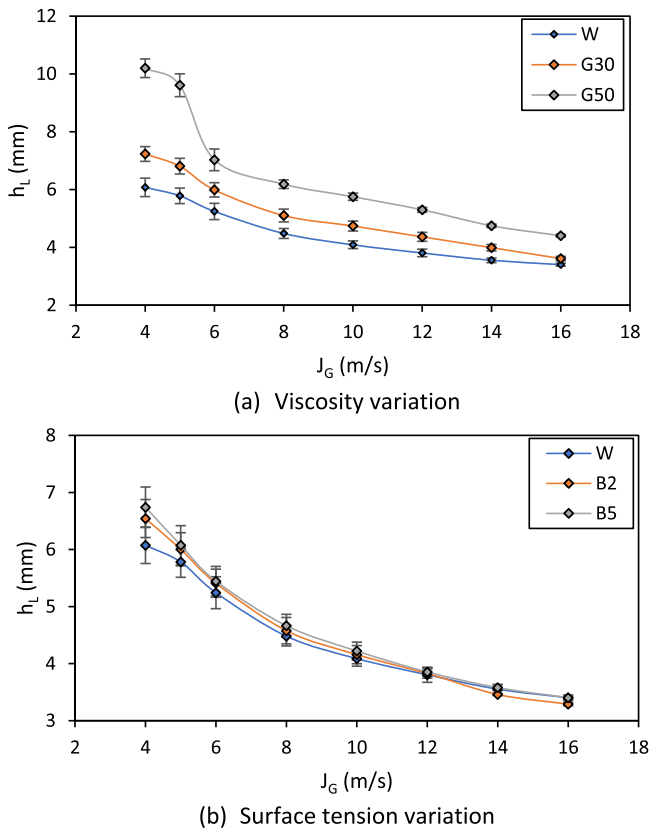
(a) Viscosity variation

(b) Surface tension variation

Fig. 10. The average of liquid film thickness with variation of J_G and liquid physical properties (viscosity and surface tension).

correlations of several previous researchers were also presented in Fig. 11 as a comparison. As shown in Fig. 10, the correlation proposed by Mantilla et al. (2009) and Setyawan and Indarto (2016) over-predicted to the data from the present experiment. The correlation proposed by Bae et al. (2017) over-predicted for most $X \geq 0.18$ and under-predicted for most $X < 0.18$ against St values from the present experimental data. The correlation proposed by Hudaya et al. (2019) was under-predicted at the value of $X < 0.05$ and the prediction is quite good for $X \geq 0.05$ against St values from the current experimental data.

From the facts of Fig. 11 above, the prediction results from the correlations of several previous researchers tend to be over/under predicted with respect to the present experimental data. This is because several parameters in the correlation are built based on the fitting process with data obtained from their respective experimental conditions (can be seen in Table 1), which is different from the present experimental conditions. Thus, it is necessary to develop a new correlation through the fitting process with the present experimental data and several previous researchers, so that it is expected to be able to predict wave frequencies in stratified flow accurately. Here, dimensional analysis using Buckingham's Pi theory is used to examine the dominant factors that influence the frequency of the waves based on experimental data. From various references regarding several factors that influence the wave frequency, the wave frequency function can be written as follows:

$$f = f(J_G,\ J_L,\ D,\ \mu_L, \mu_G,\ \rho_L, \rho_G, \sigma_L) \tag{4}$$

Moreover, a dimensional analysis was carried out using the Buckingham's Pi theory.

$$\Pi_1 = \frac{f\,D}{J_L} \tag{5}$$

$$\Pi_2 = \frac{J_G}{J_L} \tag{6}$$

$$\Pi_3 = \frac{\rho_G}{\rho_L} \tag{7}$$

$$\Pi_4 = \frac{J_L\,\rho_L\,D}{\mu_L} \tag{8}$$

$$\Pi_5 = \frac{J_L\,\rho_L\,D}{\mu_G} \tag{9}$$

$$\Pi_6 = \frac{\rho_L\,J_L^2\,D}{\sigma_L} \tag{10}$$

Through simplification with operations (multiply and or divide) between these non-dimensional parameters, the Π parameter can be simplified to:

$$\Pi_1 = f\left(\Pi_4,\ [\Pi_5.\Pi_2.\Pi_3]\ ,\ [\Pi_2.\Pi_3^2]^{1/2}.\Pi_6\right)$$

$$\frac{f\,D}{J_L} = a\left[\frac{J_L\,\rho_L\,D}{\mu_L}\right]^b \left[\frac{J_G\,\rho_G\,D}{\mu_G}\right]^c \left[\sqrt{\frac{\rho_G}{\rho_L}\left(\frac{J_G}{J_L}\right)^2}\right]^d \left[\frac{\rho_L\,J_L^2\,D}{\sigma_L}\right]^e \tag{11}$$

From the Eq. (11), the following equation is obtained:

$$St = a\ Re_L^b\ Re_G^c\ \left[\frac{1}{X}\right]^d We^e \tag{12}$$

The values of a, b, c, d, and e were searched by non-linier regression analysis using present experimental data on the RW and ED + DW sub-regimes, as well as data from Mantilla et al. (2009), Setyawan and Indarto (2016), Bae et al. (2017) and Hudaya et al (2019), resulting in the following new wave frequency correlation:

$$S_t = 0.173\left[\frac{Re_G}{Re_L}\right]^{0.049} X^{-1.176}\ We^{-0.012} \tag{13}$$

The Eq. (13) means that when the Reynold number ratio increases, the Strouhal number as a representation of wave frequency also increases. This is in accordance with the results of Hudaya et al. (2019). Meanwhile, the increase of the Martinelli parameter causes the decrease of the Strouhal number. This is in accordance with that of Mantila et al. (2009), Bae et al. (2017) and Hudaya et al. (2019). In addition, from the correlation it is noticed that an increase in the Weber number causes a decrease in the Strouhal number, although the effect is very small. The effect of the Martinelli parameter on the Strouhal number is the largest compared to the ratio of the Reynold number and Weber number. This shows that an increase in J_G has a very large effect on the frequency of the wave. An increase in J_G will cause the Martinelli parameter to decrease, hence the Strouhal number as a representation of the wave frequency will increase. This is in accordance with the experimental results shown in Table 7, where at $J_G > 8$, the wave frequency increases with the increase in J_G. In this experimental study, at the gas-liquid interface, RW and ED + DW are formed. Meanwhile, at $J_G \leq 8$ m/s the relationship between J_G and wave frequency for almost all J_L variations and the tested liquid has a complex tendency. This is caused by the appearance of the 2-D wave, 3-D wave, and PS with various shapes and time lag with low frequency. Thus, the correlation to predict the wave frequency proposed from this study (Eq. (13)) is more accurate to be applied to the RW and ED + DW sub-regimes. The development of the correlation that is able to predict wave frequencies more accurately to be applied to 2-D waves, 3-D waves and PS requires further research and study.

The proposed correlation from this study is then compared with the experimental results to find out how the level of correspondence between the predicted results and the experimental results. Fig. 12 shows that the proposed correlation has a good agreement with the experimental data. Most of the data appears to be spread at approximately 30% error value. To confirm the difference between the predicted and experimental values, further quantitative analysis was carried out in the

Table 7

Effect of J_G, liquid viscosity and liquid surface tension on the wave frequency.
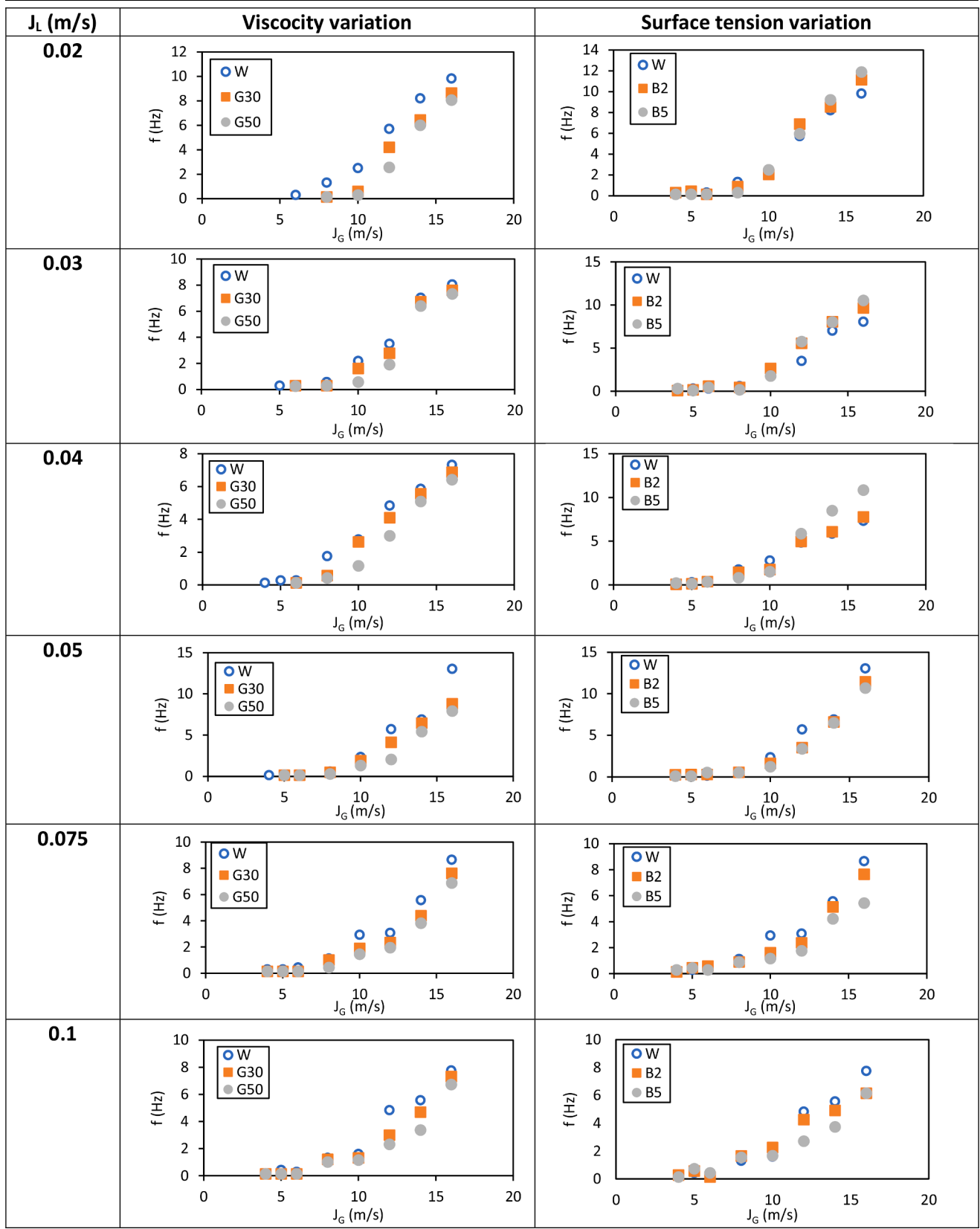
Fig. 11. Comparison of wave frequency from the results of the present study with previous works.

Fig. 12. The comparison of Eq. (13) with that of the obtained data from the present work and previous researchers.

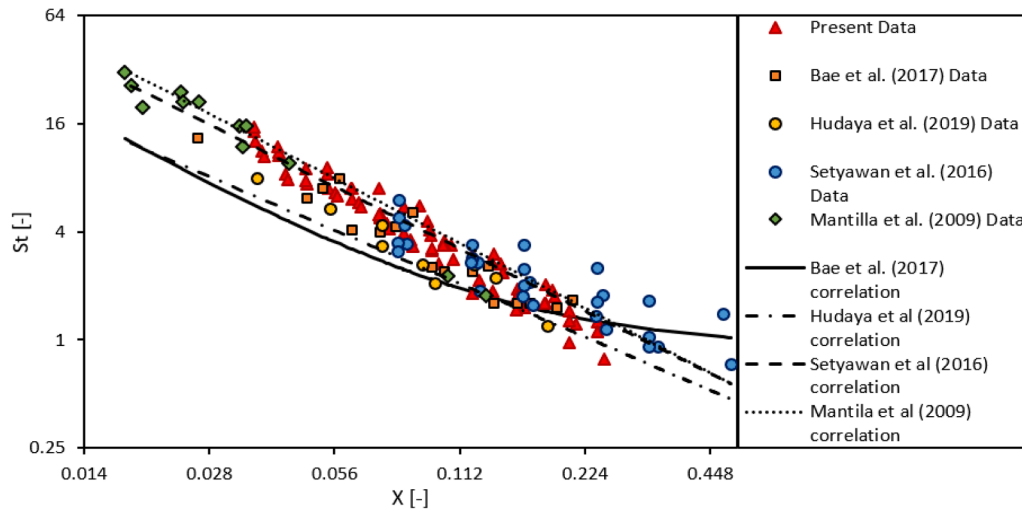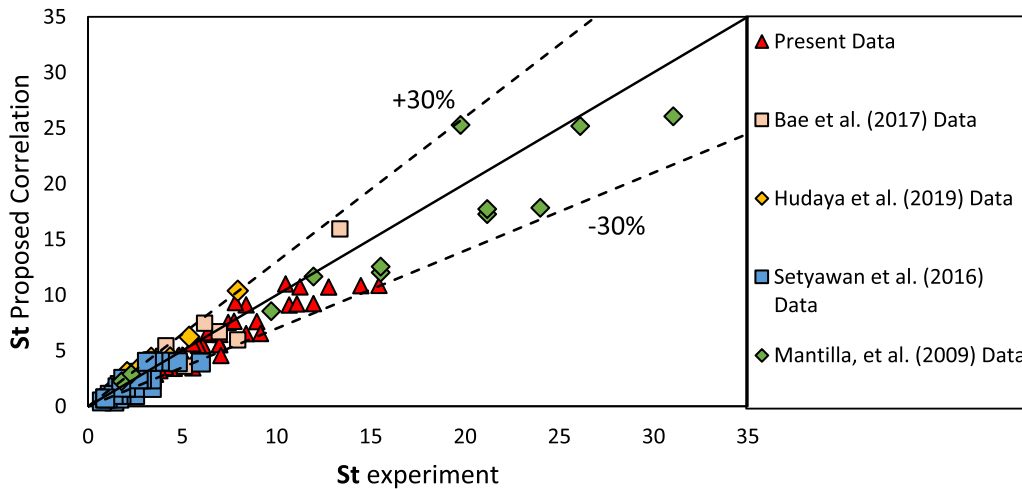form of a measurement of the mean absolute percentage error (MAPE) as follows:

$$MAPE = \frac{1}{n} \sum_{i=1}^{n} \left| \frac{St_{prediction,i} - St_{experiment,i}}{St_{experiment,i}} \right| \times 100\% \quad (14)$$

The MAPE value of the proposed correlation with experimental data from this study is 14.23%. Meanwhile, the MAPE value of the proposed correlation with data from Mantilla et al. (2009), Setyawan and Indarto (2016), Bae et al. (2017) and Hudaya, et al (2019) were 18.08%, 27.16%, 16.74% and 21.43%, respectively. The MAPE value of the correlation proposed in this study with the overall experimental data of the present and those of previous researchers is 19.53%. Meanwhile, the correlation proposed by Mantilla et al. (2009), Setyawan and Indarto (2016), Bae et al. (2017) and Hudaya et al (2019) with the overall experimental data are 31.54, 25.09, 32.53 and 30.3%. The MAPE value of the proposed correlation is currently the smallest compared to the correlation proposed by previous researchers.

5. The wave velocity

The effect of J_G on the wave velocity under the variation of J_L with the tested liquid of **W, G30, G50, B2** and **B5** is shown in Table 8. At $J_G \leq$ 8 m/s the relationship between J_G and wave velocity for almost all J_L

variations and the tested liquid has a complex tendency. This is due to the appearance of 2-D waves, 3-D waves and PS with varying shapes and time lags with low frequencies. From the entire J_L range in this experiment, at J_G more than 8 m/s, the wave velocity tends to increase regularly as J_G increases. This is because the breaking of waves was more dominant than the merging of waves. In this experimental condition, a small RW and ED + DW were formed at the interface. From Table 8 it can be seen that the wave velocity decreases with the increase of liquid viscosity. This was due to the increase in the stabilizing effect of increasing the viscosity of the liquid, so that more energy was required to drive the wave motion. This was in accordance with the results of Setyawan and Indarto (2016) who suggested that increasing the viscosity of the liquid causes a decrease in wave velocity. At $J_L \leq 0.04$ m/s and $J_G = 8$ m/s to 16 m/s, the wave velocity decreases with the decrease of liquid surface tension. Meanwhile, at $J_L = 0.05$ m/s to 0.075 m/s and $J_G = 16$ m/s, and $J_L = 0.1$ m/s with $J_G = 14$ m/s and 16 m/s, the wave velocity increases with the decrease of liquid surface tension. This was because, at low J_L, the formed waves were small, so the lower of the liquid surface tension causes the waves to decay more easily due to the impulse of the air flow. On the other hand, at high J_L, larger waves are formed, so the lower of the liquid surface tension causes the waves to move faster due to a large enough airflow.

Several researchers have proposed the correlations to predict the wave velocity in gas-liquid two-phase flow as summarized in Table 1.

Table 8

Effect of J_G, liquid viscosity and liquid surface tension on wave velocity.

J_L (m/s)	Viscosity variation	Surface tension variation
0.02		
0.03		
0.04		
0.05		
0.075		
0.1		
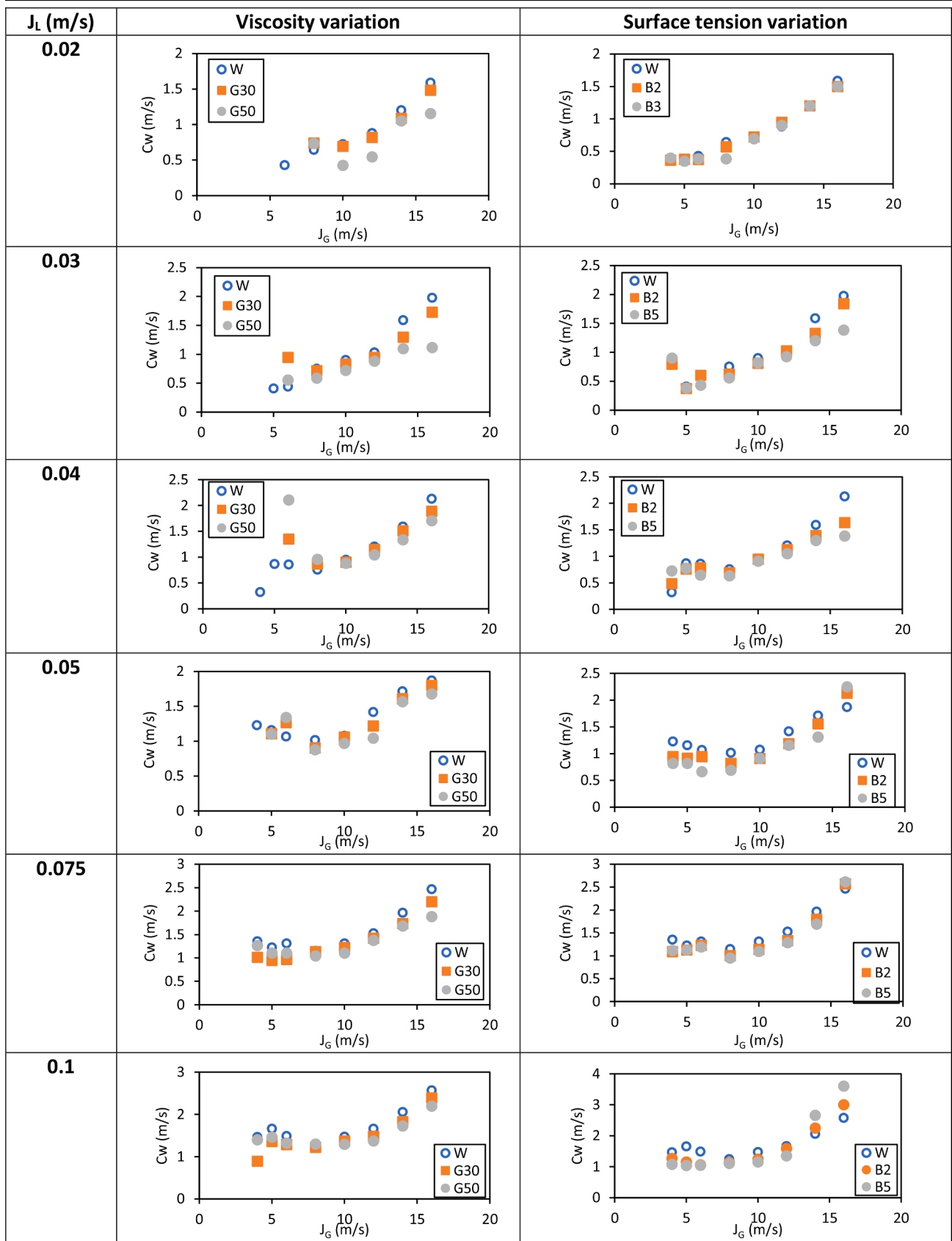
Fig. 13. Comparison of wave velocity from the results of the present study with previous works.

However, correlations to predict wave velocity in stratified flow by experimentation using variations in viscosity and liquid surface tension have not been studied. The correlation proposed by the previous researchers used the nondimensional parameters X (mod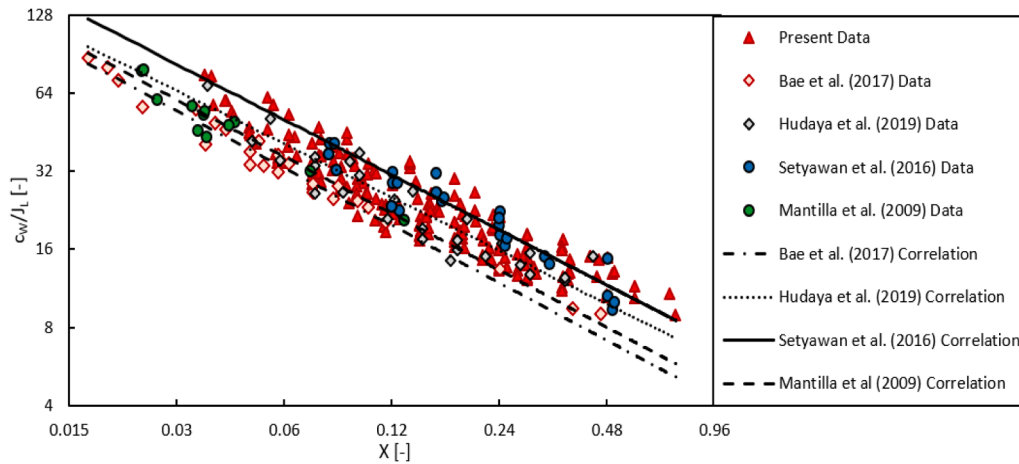ified Martinelli parameter) and c_w/J_L to predict the wave velocity. Fig. 13 illustrates the comparison of experimental data from the present study and those of previous researchers. From the X vs c_w/J_L graph, it was shown that the data from the current experiment and the previous researchers show the same trend, whereas the Martinelli parameter increases, the c_w/J_L decreases. The proposed correlation of several previous researchers was also applied in Fig. 12 as a comparison. As shown in Fig. 13, the correlation of Setyawan and Indarto (2016) slightly over-predicted to the experimental data under the flow condition of the value of X ≤ 0.12. The correlation of Mantila et al. (2009) and Bae et al. (2017) slightly under-predicted for most of the X values with respect to c_w/J_L from the data from the current experiment. Hudaya et al. (2019) correlation resulted in quite good predictions for the value of X less than or equal to 0.24 and under-predicted for the value of X more than 0.24 with respect to c_w/J_L from the data from the current experimental results.

From the facts of Fig. 13, further analysis needs to be developed to formulate a correlation to predict the wave velocity of stratified flow accurately. Here, dimensional analysis was carried out as previously applied to wave frequencies. The influential variables and dimensions for the wave velocity in this study were the same as the wave frequency. Thus, it is possible to construct a dimensionless six Pi parameter (Π) by analysis of Buckingham's Pi theory. D, J_L and L were selected as repeating variables. The dimensionless parameters are expressed as follows:

$$\Pi_1 = \frac{c_w}{J_L} \tag{15}$$

$$\Pi_2 = \frac{J_G}{J_L} \tag{16}$$

$$\Pi_3 = \frac{\rho_G}{\rho_L} \tag{17}$$

$$\Pi_4 = \frac{J_L \rho_L D}{\mu_L} \tag{18}$$

$$\Pi_5 = \frac{J_L \rho_L D}{\mu_G} \tag{19}$$

$$\Pi_6 = \frac{\rho_L J_L^2 D}{\sigma_L} \tag{20}$$

The same steps are taken as in the preparation of the non-

dimensional wave frequency parameters so that the general form of the parameter function can be written as follows:

$$\Pi_1 = f\left(\Pi_4, \ [\Pi_5.\Pi_2.\Pi_3] \ , \ [\Pi_2.\Pi_3^2]^{1/2}.\Pi_6\right)$$

$$\frac{c_w}{J_L} = a\left[\frac{J_L \rho_L D}{\mu_L}\right]^b \left[\frac{J_G \rho_G D}{\mu_G}\right]^c \left[\sqrt{\frac{\rho_G}{\rho_L}\left(\frac{J_G}{J_L}\right)^2}\right]^d \left[\frac{\rho_L J_L^2 D}{\sigma_L}\right]^e \tag{21}$$

$$\frac{c_w}{J_L} = a \ Re_L^b \ Re_G^c \left[\frac{1}{X}\right]^d We^e$$

Values of a, b, c, d, dan e are searched by non-liner regression analysis using current experimental data, as well as data from Mantilla et al. (2009), Setyawan and Indarto (2016), Bae et al. (2017), and Hudaya et al (2019), resulting in the following wave velocity correlation:

$$\frac{c_w}{J_L} = 5.853 \left[\frac{Re_G}{Re_L}\right]^{-0.017} X^{-0.734} We^{0.064} \tag{22}$$

The Eq. (22) means that the increase of the Reynold number ratio causes the decrease of the ratio of the wave velocity and J_L, although the effect is very small. The increase of the Martinelli parameter causes the decrease of the ratio of wave velocity and J_L with a large enough effect. This is in accordance with the results of the study of Hudaya et al. (2019). Meanwhile, the increase in Weber number causes the ratio of wave velocity and J_L to increase although the effect is small. The effect of the Martinelli parameter on the ratio of wave velocity and J_L is the largest compared to the Reynold number and Weber number ratios. This shows that the increase in J_G has a large enough effect on the increase in wave velocity. An increase in J_G will cause the Martinelli parameter to decrease, so the ratio of wave velocity and J_L will increase. This is in accordance with the experimental results shown in Table 8, where at J_G > 8, the wave velocity increases with the increase in J_G. In this experimental study, at the gas-liquid interface, RW and ED + DW are formed. Meanwhile, at J_G ≤ 8 m/s the relationship between J_G and wave velocity for almost all J_L variations and the tested liquid has a complex tendency. This is caused by the appearance of the 2-D wave, 3-D wave, and PS with various shapes and time lag with low frequency. Thus, the correlation to predict wave velocity proposed from this study (Eq. (22)) is more accurate to be applied to the RW and ED + DW sub-regimes. The development of the correlation that is able to predict wave velocity more accurately to be applied to 2-D waves, 3-D waves and PS requires further research and study.

The proposed correlation (Eq. (22)) from the present study is then compared with the experimental results to find out how the level of correspondence between the predicted results and the experimental
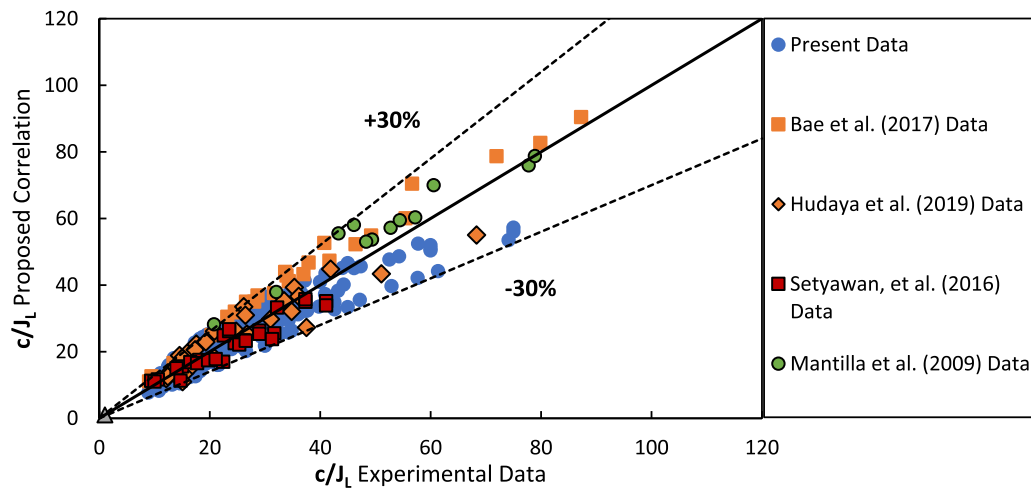
Fig. 14. The comparison of Eq. (22) with that of the obtained data from the present work and previous researchers.

results. Fig. 14 shows that the proposed correlation has a good match with the experimental data. Most of the data appear to be spread at approximately 30% error value. To confirm the difference between the predicted and experimental values, further quantitative analysis was carried out in the form of a measurement of the mean absolute percentage error (MAPE). The MAPE value of the proposed correlation with experimental data from the present study is 13.85%. Meanwhile, the MAPE value of the proposed correlation with data from Mantilla et al. (2009), Setyawan and Indarto (2016), Bae et al. (2017) and Hudaya et al (2019) are 13.88%, 11.7%, 20.94%, and 14.18%. The MAPE value of the correlation proposed in this study with the overall experimental data of the present and those of previous researchers is 14.91%. Meanwhile, the correlation proposed by Mantilla et al. (2009), Setyawan and Indarto (2016), Bae et al. (2017) and Hudaya et al. (2019) are 16.68%, 31.43%, 21.48% and 17.2%. The MAPE value of the proposed correlation is currently the smallest compared to the correlation proposed by previous researchers. This shows that the proposed correlation from the results of this study more accurately predicts the frequency of stratified flow waves compared to the correlation proposed by previous researchers.

6. Conclusion

The effect of the liquid physical properties on liquid film thickness, wave frequency, and wave velocity of co-current gas-liquid stratified two-phase flow have been studied in this research using image processing techniques. The characteristics of each flow sub-regime were analyzed using a probability distribution function (PDF) and discrete wavelet transform (DWT) based on time series data of liquid film thickness. In addition, the time-series data of the liquid film thickness was analyzed using power spectral density (PSD) to obtain wave frequency and cross-correlation to obtain wave velocity. The results are summarized as follows:

a Based on the stratified flow sub-regime maps, the increase of the liquid viscosity and the decrease of the liquid surface tension cause the transition line from RW to ED + DW to shift to a lower both JL and JG. The increase of the liquid viscosity causes the decrease of the RW region and increases the S, PS, and ED + DW regions, while the decrease of the liquid surface tension causes the decrease of the PS region, eliminates the S region, and increases the 2-D and 3-D wave regions.

b In the RW and ED + DW sub-regimes, the increase of the liquid viscosity causes the wavelet energy to shift to a larger scale and a lower frequency, while the decrease of the liquid surface tension has no effect on the scale and frequency shift of the wavelet energy. The

increase of the liquid viscosity causes an increase in the liquid film thickness. Meanwhile, the surface tension variation has a very small effect on the liquid film thickness.

c Superficial gas velocity (JG), liquid viscosity and liquid surface tension are important parameters in developing correlations to predict void fraction, interfacial shear stress and pressure gradient as future research work.

d In the 2-D wave, 3-D wave and PS sub-regimes, the relationship between JG with wave frequency and wave velocity is quite complex. Meanwhile, in the RW and ED + DW sub-regimes, the frequency and velocity of the waves tend to increase with increasing JG.

e The new correlations to predict the frequency and velocity of the interfacial waves in co-current gas-liquid stratified two-phase flow have been developed with the MAPE of the correlation of wave frequency and velocity of 19.53% and 14.91%, respectively.

CRediT authorship contribution statement

Setya Wijayanta: Conceptualization, Methodology, Investigation, Writing – original draft, Formal analysis. **:** Formal analysis, Data curation, Writing – review & editing, Resources, Funding acquisition, Supervision. **:** Resources, Funding acquisition, Writing – review & editing, Supervision. **Ari Prasetyo:** Methodology, Investigation, Formal analysis. **Akhmad Zidni Hudaya:** Methodology, Investigation, Formal analysis.

Declaration of Competing Interest

The authors declare that they have no known competing financial interests or personal relationships that could have appeared to influence the work reported in this paper.

Data Availability

Data will be made available on request.

Acknowledgments

References

Al-Sarkhi, A., Sarica, C., Magrini, K., 2012. Inclination effects on wave characteristics in annular gas–liquid flows. AIChE J. 58 (4), 1018–1029.

Al-Wahaibi, T., Angeli, P., 2011. Experimental study on interfacial waves in stratified horizontal oil-water flow. Int. J. Multiph. Flow 37, 930–940.

Andritsos, N., Hanratty, T.J., 1987. Interfacial instabilities for horizontal gas-liquid flows in pipelines. Int. J. Multiph. Flow 13 (5), 583–603. https://doi.org/10.1016/0301-9322(87)90037-1.

Aydin, T.B., Torres, C.F., Karami, H., Pereyra, E., Sarica, C., 2015. On the characteristics of the roll waves in gas–liquid stratified-wavy flow: a two-dimensional perspective. Exp. Therm. Fluid Sci. 65, 90–102.

Bae, B., Ahn, T., Jeong, J., Kim, K., Yun, B., 2017. Characteristics of an interfacial wave in a horizontal air-water stratified flow. Int. J. Multiph. Flow 97, 197–205. https://doi.org/10.1016/j.ijmultiphaseflow.2017.08.009.

Bruno, Kenneth, 1988. A Study of Interfacial Waves in Gas-Liquid Flows. The University of Notre Dame. Ph.D. Dissertation.

Catrawedarma, I.G.N.B., Deendarlianto, Indarto, 2021. Statistical characterization of flow structure of air-water two-phase flow in airlift pump-bubble generator system. Int. J. Multiph. Flow 138 (2), 1–16.

Chen, X.T., Cai, X.D., Brill, J.P., 1997. Gas-liquid stratified-wavy flow in ihorizontal pipelines. J. Energy Resour. Technol. 119 (4), 209–216. https://doi.org/10.1115/1.2794992. *Transactions of the ASME*.

Dinaryanto, O., Prayitno, Y.A.K., Majid, A.I., Hudaya, A.Z., Nusirwan, Y.A., Widyaparaga, A., Indarto, Deendarlianto, 2017. Experimental investigation on the initiation and flow development of gas-liquid slug two-phase flow in a horizontal pipe. Exp. Therm. Fluid Sci. 81, 93–108. https://doi.org/10.1016/j.expthermflusci.2016.10.013.

Dukler, A.E., Hubbard, M.G., 1975. A model for gas-liquid slug flow in horizontal and near horizontal tubes. Ind. Eng. Chem. Fundam. 14 (4), 337–346.

Elperin, T., Klochko, M., 2002. Flow regime identification in a two-phase flow using wavelet transform. Exp. Fluids 32 (11), 674–682. https://doi.org/10.1007/s00348-002-0415-x.

Fernandino, M., Ytrehus, T., 2006. Determination of flow sub-regimes in stratified air-water channel flow using LDV spectra. Int. J. Multiph. Flow 32 (4), 436–446. https://doi.org/10.1016/j.ijmultiphaseflow.2006.01.003.

Gawas, K., Karami, H., Pereyra, E., Al-Sarkhi, A., Sarica, C., 2014. Wave characteristics in gas-oil two phase flow and large pipe diameter. Int. J. Multiph. Flow 63, 93–104. https://doi.org/10.1016/j.ijmultiphaseflow.2014.04.001.

Govier, G.W., Omer, M.M., 1962. The horizontal pipeline flow of air-water mixtures. Can. J. Chem. Eng. 40 (3), 93–104. https://doi.org/10.1002/cjce.5450400303.

Hanratty, T.J., Hershman, A., 1961. Initiation of roll waves. AIChE J. 7 (3), 488–497. https://doi.org/10.1002/aic.690070330.

Hudaya, A.Z., Widyatama, A., Dinaryanto, O., Juwana, W.E., Indarto, Deendarlianto, 2019. The liquid wave characteristics during the transportation of air-water stratified co-current two-phase flow in a horizontal pipe. Exp. Therm. Fluid Sci. 103 (July 2018), 304–317. https://doi.org/10.1016/j.expthermflusci.2019.01.021.

Kowalski, J.E., 1987. Wall and interfacial shear stress in stratified flow in a horizontal pipe. AIChE J. 33 (2), 583–603.

Kuntoro, H.Y., Hudaya, A.Z., Dinaryanto, O., Majid, I., 2016. An improved algorithm of image processing technique for film thickness measurement in a horizontal stratified gas- liquid two-phase flow. AIP Conf. Proc. 1737, 040010 https://doi.org/10.1063/1.4949298.

Lin, P.Y., Hanratty, T.J., 1986. Prediction of the initiation of slugs with linear stability theory. Int. J. Multiph. Flow 12 (1), 79–98. https://doi.org/10.1016/0301-9322(86)90005-4.

Lin, P.Y., Hanratty, T.J., 1987. Effect of pipe diameter on flow patterns for air-water flow in horizontal pipes. Int. J. Multiph. Flow 13 (4), 549–563.

Lockhart, R.W., Martinelli, R.C., 1949. Proposed correlation of data for isothermal two-phase, two-component flow in pipes. Chem. Eng. Prog. 45, 39–48.

Mallat, S.G., 1989. Multiresolution approximations and wavelet orthonomal bases of $L^2(R)$. In: Trans. Am. Math. Soc., 315, pp. 69–87.

Mandhane, 1974. A flow pattern map for gas-liquid in horizontal piper. Int. J. Multiph. Flow 1, 537–553.

Mantilla, I., Viana, F., Kouba, G., Roberts, R., 2009. Experimental investigation of liquid entrainment in gas at high pressure. In: Proceedings of the ASME Fluids Engineering Division Summer Meeting, FEDSM, pp. 211–225.

Matsubara, H., Naito, K., 2011. Effect of liquid viscosity on flow patterns of gas-liquid two-phase flow in a horizontal pipe. Int. J. Multiph. Flow 37 (10), 1277–1281.

McCready, M.J., Hanratty, T.J., 1985. Effect of air shear on gas absorption by a liquid film. AIChE J. 31, 2066–2074.

Setyawan, A., Indarto, Deendarlianto, 2016. The effect of the fluid properties on the wave velocity and wave frequency of gas-liquid annular two-phase flow in a horizontal pipe. Exp. Therm. Fluid Sci. 71, 25–41. https://doi.org/10.1016/j.expthermflusci.2015.10.008.

Spedding, P.L., Nguyen, V.T., 1979. Regime maps for air water two phase flow. Chem. Eng. Sci. 35 (4), 779–793. https://doi.org/10.1016/0009-2509(80)85062-7.

Taitel, Y., A.E, Dukler, 1976. A model for predicting flow regime transitions in horizontal and near horizontal gas-liquid flow. AIChE J. 22 (1), 47–55.

Villarreal, J., Laverde, D., Fuentes, C., 2006. Carbon-steel corrosion in multiphase slug flow and CO_2. Corros. Sci. 48 (9), 2363–2379. https://doi.org/10.1016/j.corsci.2005.09.003.

Wijayanta, S., Indarto, Deendarlianto, Catrawedharma, I.G.N.B., Hudaya, A.Z, 2022. Statistical characterization of the interfacial behavior of the sub-regimes in gas-liquid stratified two-phase flow in a horizontal pipe. Flow Meas. Instrum. 83, 1–19. https://doi.org/10.1016/j.flowmeasinst.2021.102107.